Challenges for Polarimetry at the ILC

Moritz Beckmann, Anthony Hartin, Jenny List

DESY - FLC

EUCARD Workshop
"Spin optimization at Lepton accelerators"

Mainz, Germany
February 12, 2014

Outline

- Introduction
  - Polarimetry in the ILC beam delivery system
  - Spin transport
- Results
  - Beamline simulation
  - Collision effects
    - Polarization measurement at the disrupted beam
    - Beamline design in view of the polarization measurement
    - Impact of the laser spot size at the downstream polarimeter

ILC Beam Delivery System (BDS)

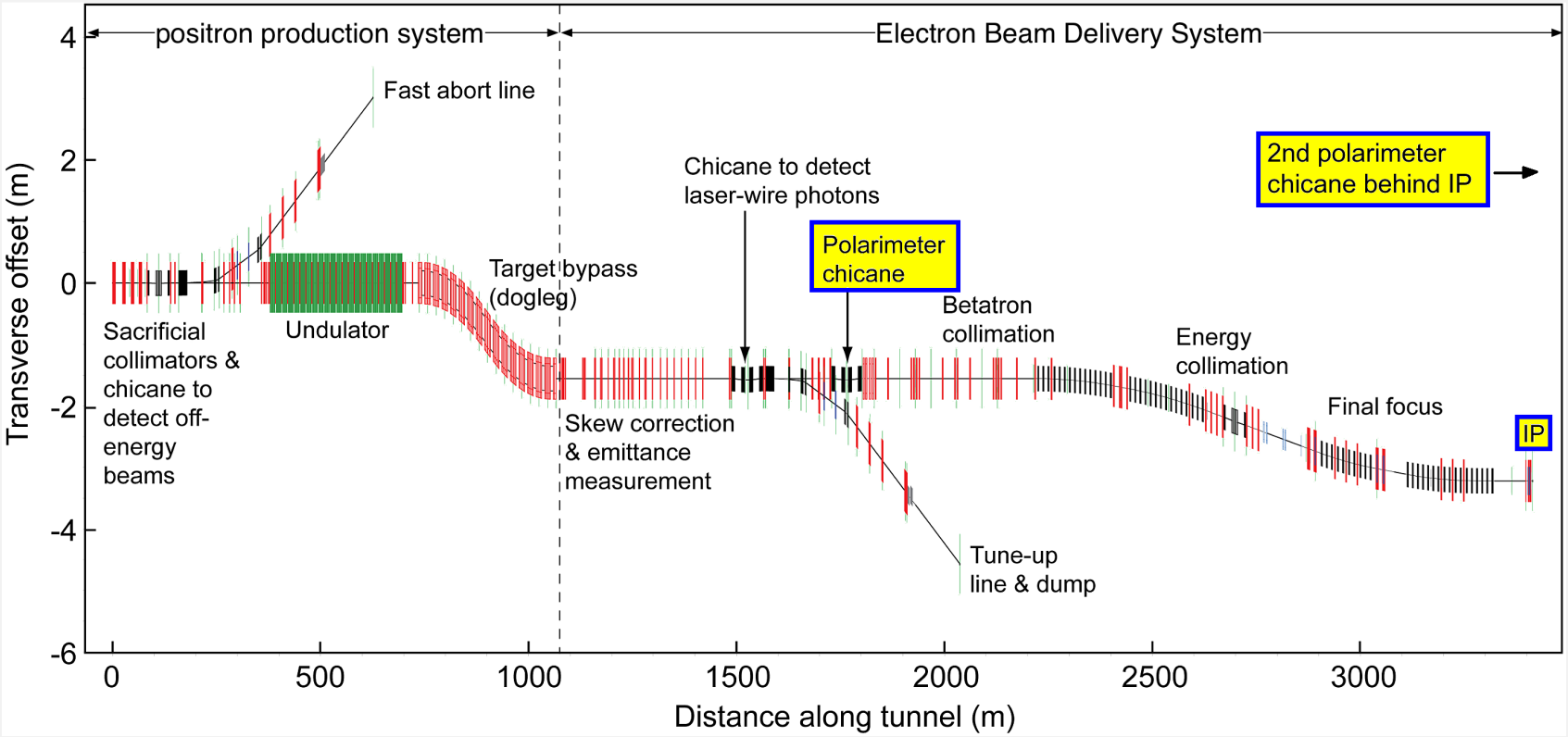

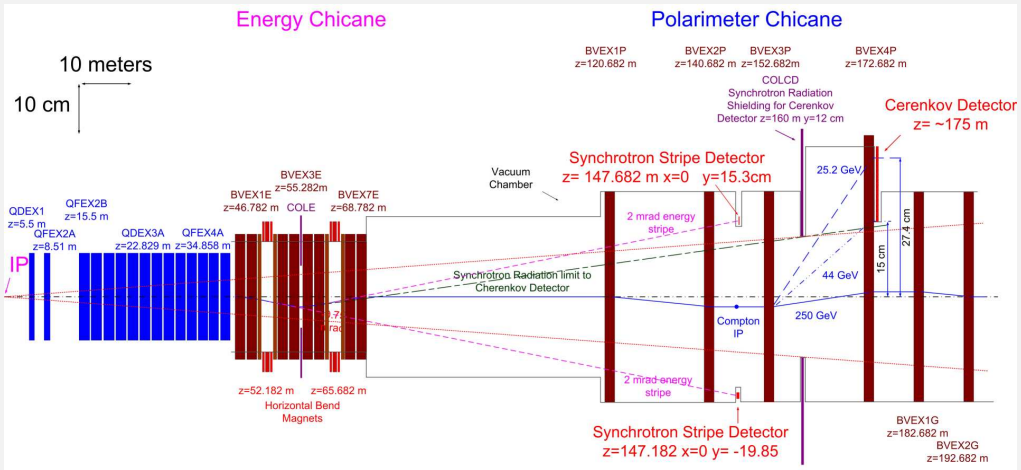

Laser Compton Polarimeter (Principle)

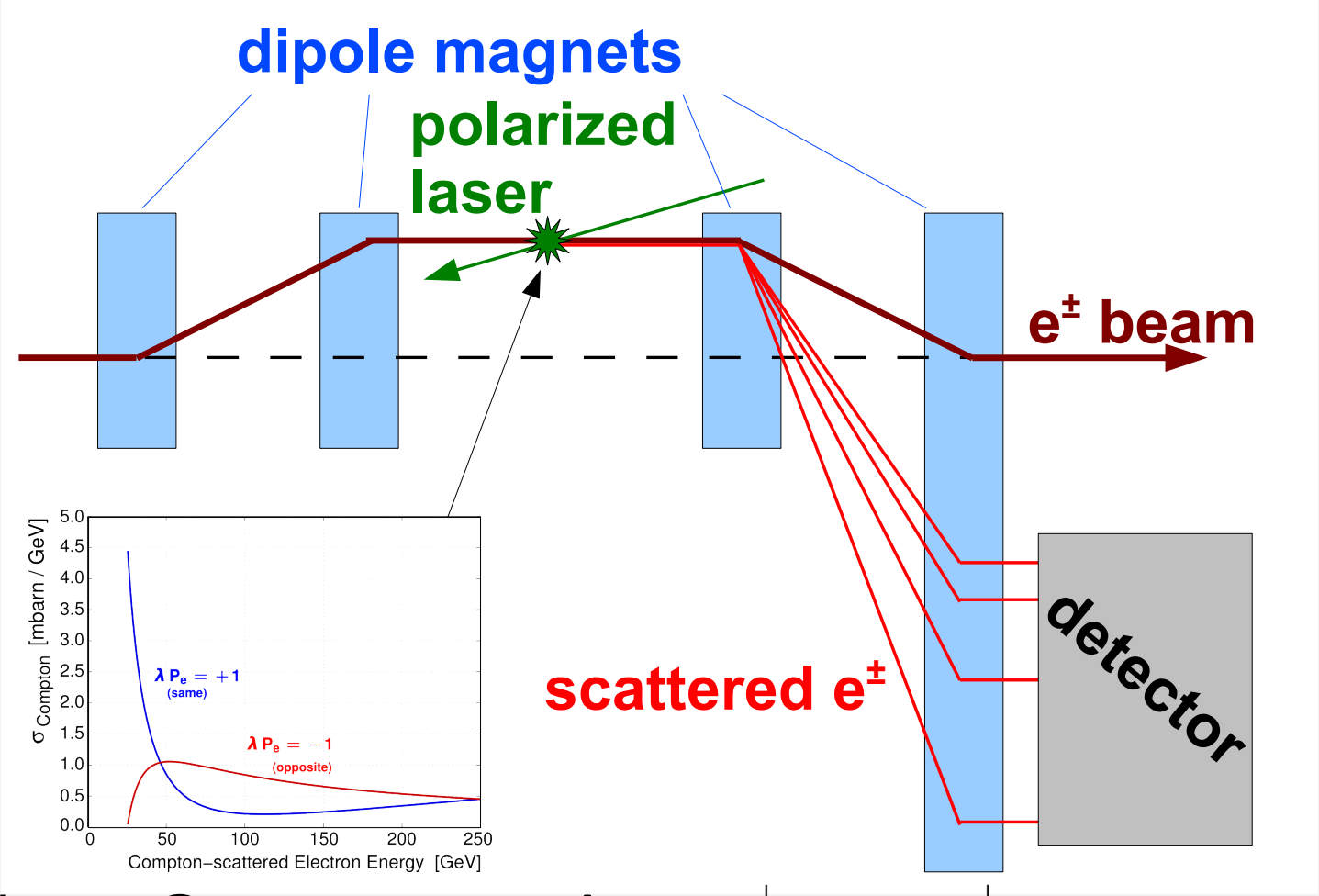

- Laser: **Compton scattering** $e^{\pm}\gamma \rightarrow e^{\pm}\gamma$
- Scattering **cross section depends on** $\mathcal{P}_z$
- Magnet chicane separates scattered $e^{\pm}$ from beam
- $\mathcal{P}_z$ is determined from scattered electrons

Polarimetry at the ILC

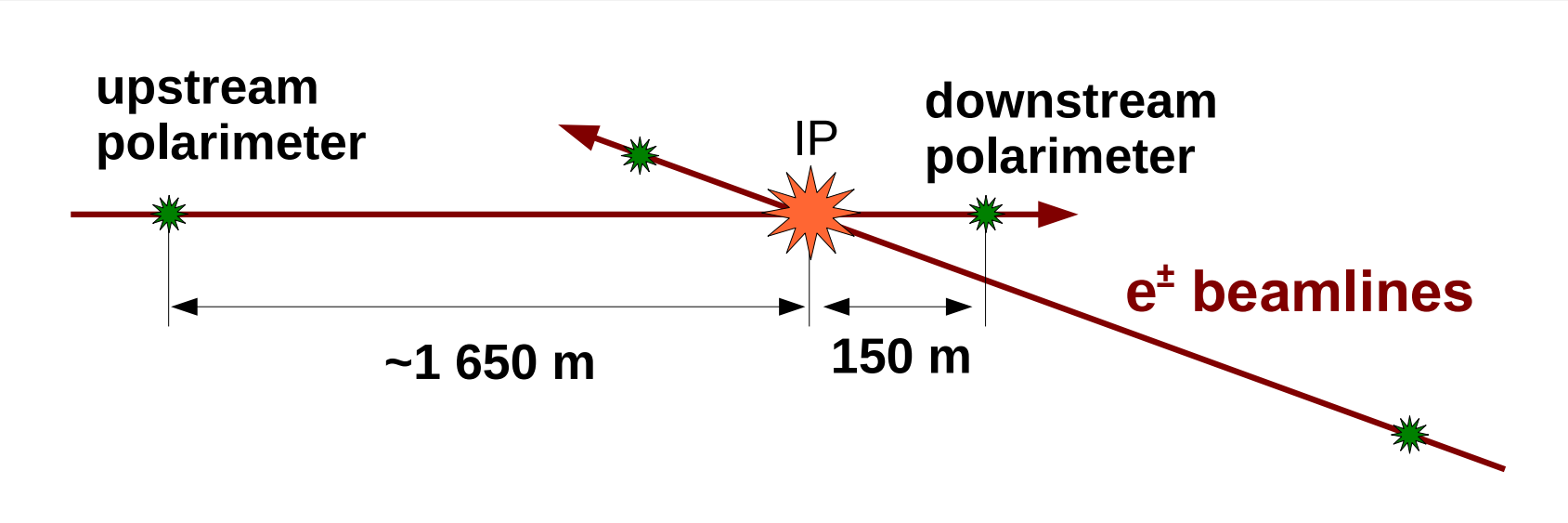

- Two Compton polarimeters per beam to measure $\mathcal{P}_z$
  - Upstream polarimeter undisturbed by collision effects
  - Downstream polarimeter assesses collision effects
  - 0.25 % systematic uncertainty (goal)
- **What do these measurements tell us about the longitudinal polarization at the IP?**

Polarimetry at the ILC

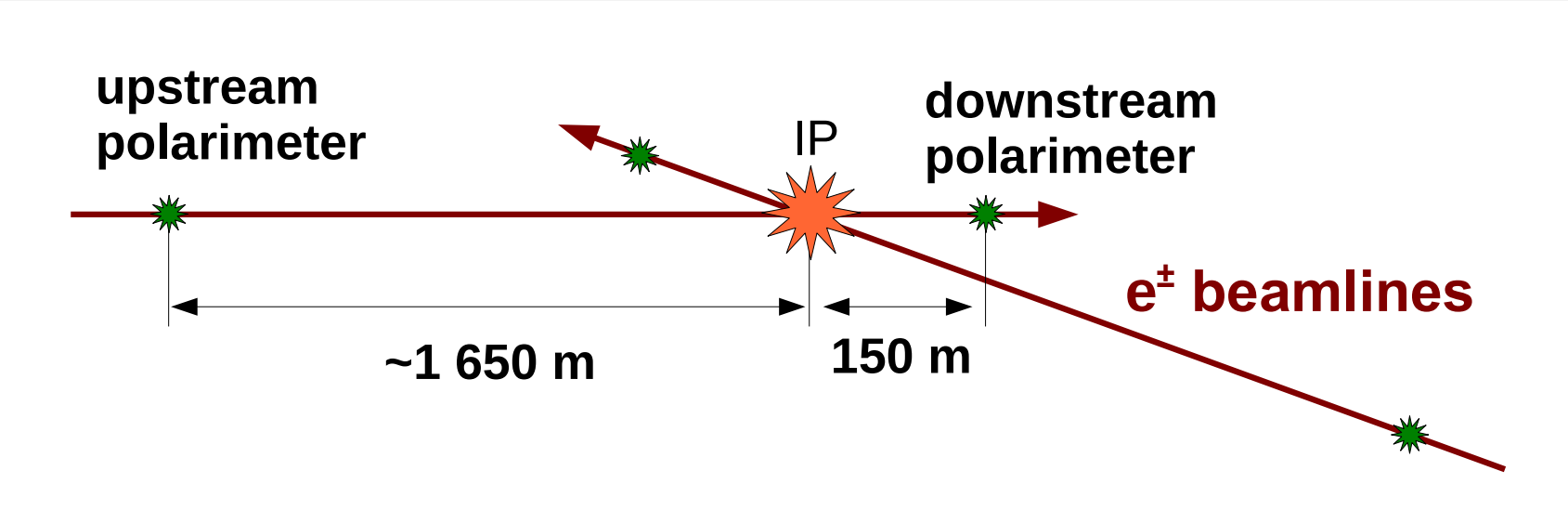

- Two Compton polarimeters per beam to measure $\mathcal{P}_z$
  - Upstream polarimeter undisturbed by collision effects
  - Downstream polarimeter assesses collision effects
  - 0.25 % systematic uncertainty (goal)
- **What do these measurements tell us about the longitudinal polarization at the IP?**
  $\rightarrow$ spin transport simulation
- Aim to understand spin transport to 0.1 %

Spin Precession

- Spin precession in electromagnetic fields: **T-BMT** equation
- For $\vec{B}_\perp$ only:

$$\vartheta_{\text{spin}} = \mathbf{b(E)} \cdot \vartheta_{\text{orbit}}$$

$$b(E) = a\gamma + 1 = \frac{g-2}{2} \cdot \frac{E}{m} + 1$$
$$\approx \mathbf{568} \quad \text{for } 250\,\text{GeV-electrons}$$

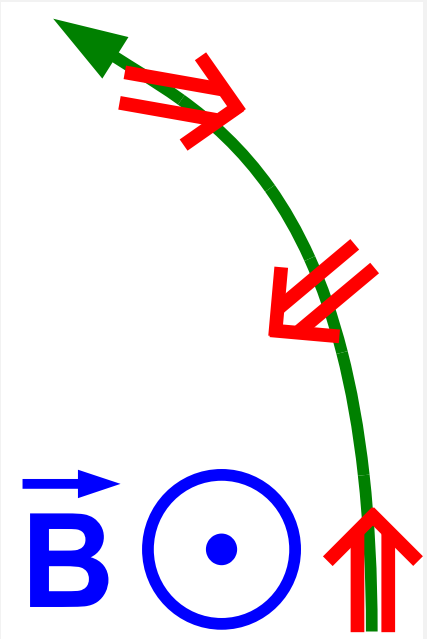

- Dipole magnets, no beam energy spread: spin vectors precess uniformly, $|\vec{\mathcal{P}}|$ conserved

Spin Fan-Out in Quadrupole Magnets

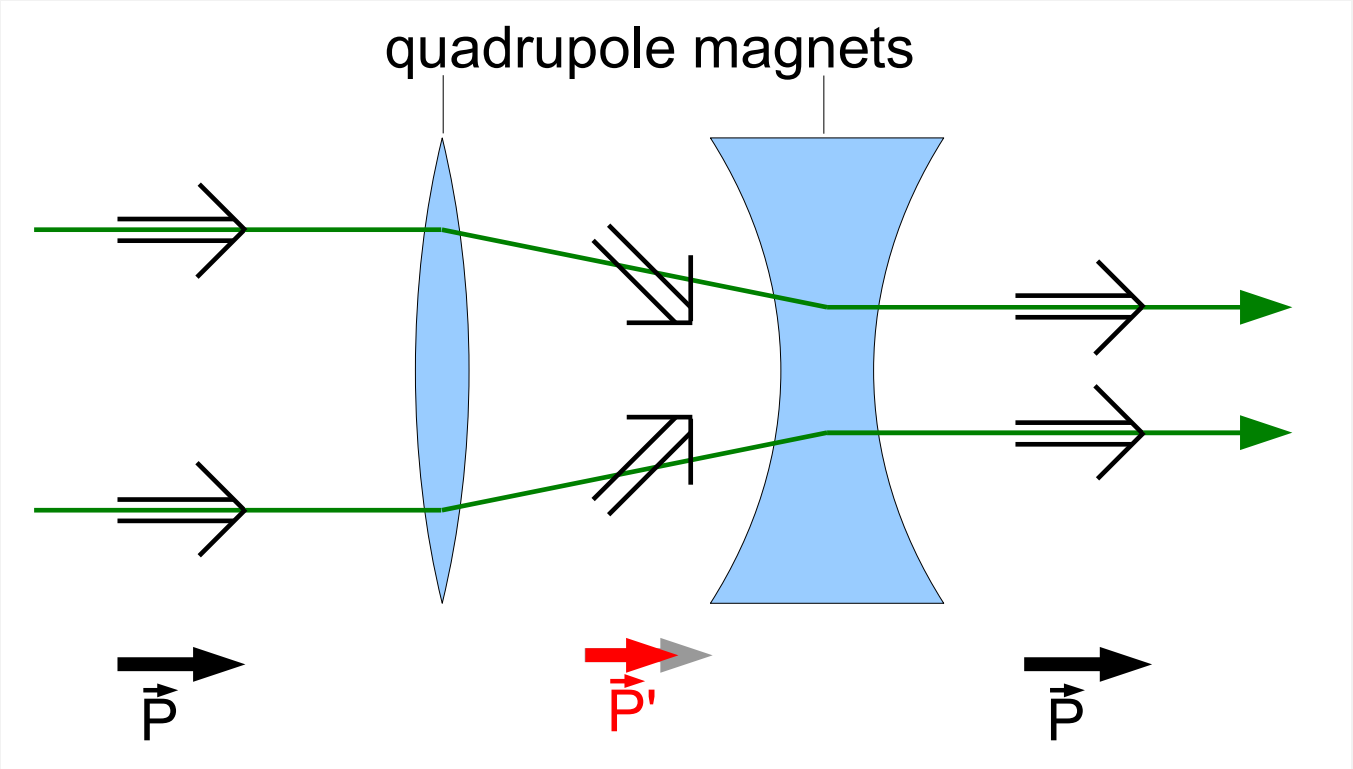

For illustration purposes, the second quadrupole is stronger. Two-dimensional betatron oscillations are not taken into account here.

- Different precession angles after first quadrupole
  $\Rightarrow$ polarization $|\vec{\mathcal{P}}|$ decreases
- $|\vec{\mathcal{P}}|$ recovered by second quadrupole

Beam-Beam Collision Effects

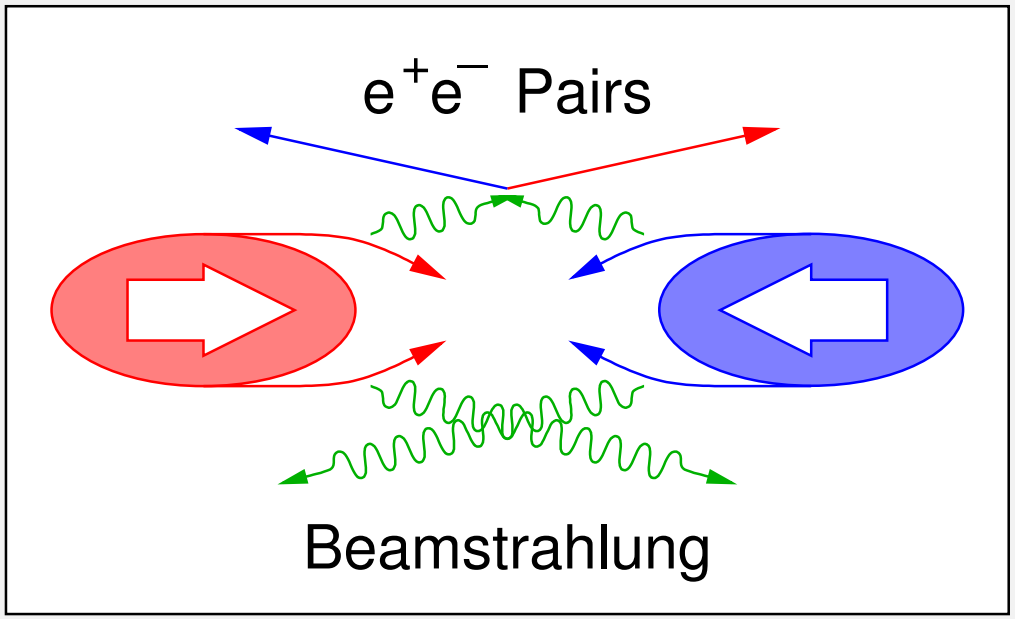

A. Vogel

Bunches focus each other by their electromagnetic fields:

- **Spin fan-out** (like in quadrupole magnets)
- **Spin flip** by emission of **beamstrahlung** (Sokolov-Ternov effect)

Spin Transport Simulation Framework

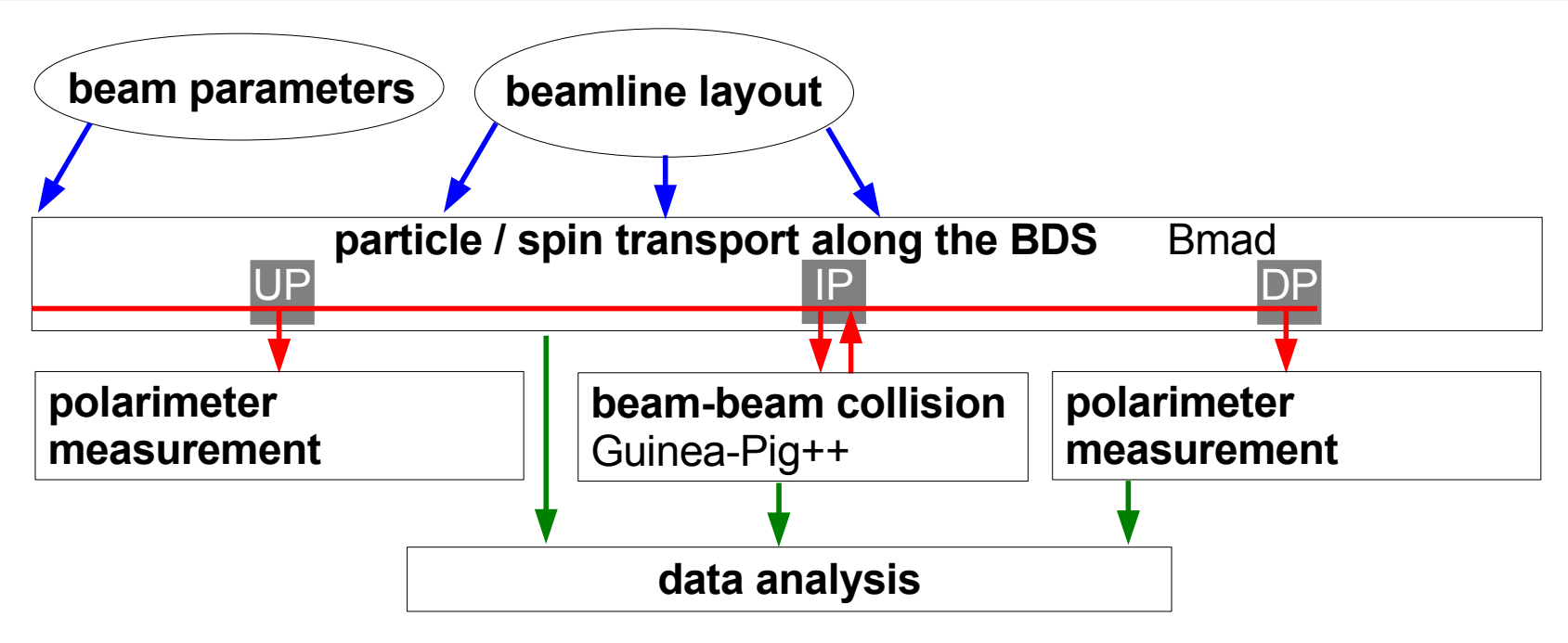

- Developed a beamline simulation (based on Bmad)
- Simulate 40 000 (macro)particles per bunch, generated from beam parameters at the beginning of the BDS
- Interfaced directly to the simulation of the collisions (Guinea-Pig++)

Results

- $\sqrt{s} = 500\,\mathrm{GeV}$
- Beam parameters according to Reference Design Report (RDR, 2007)
- Collision effects also for beam parameters according to Technical Design Report (TDR, 2013)

Spin Transport in the BDS: Basic Configuration

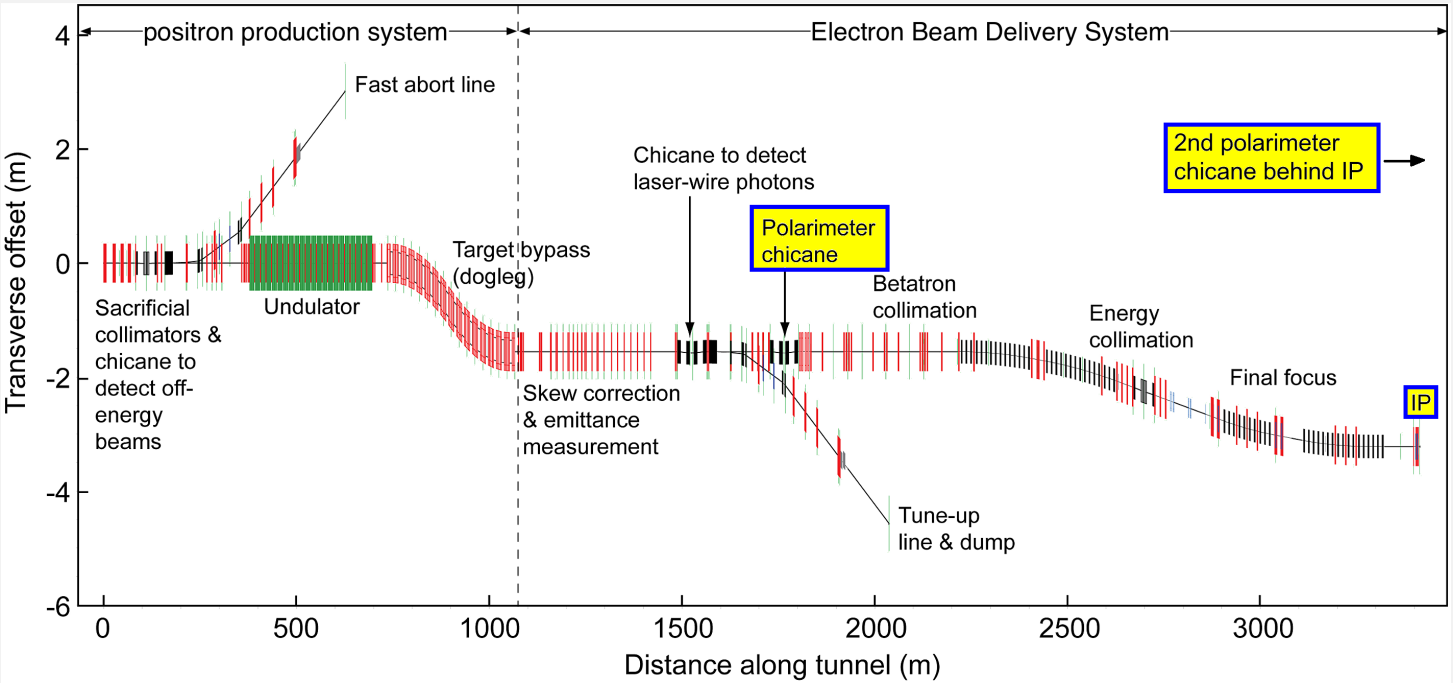

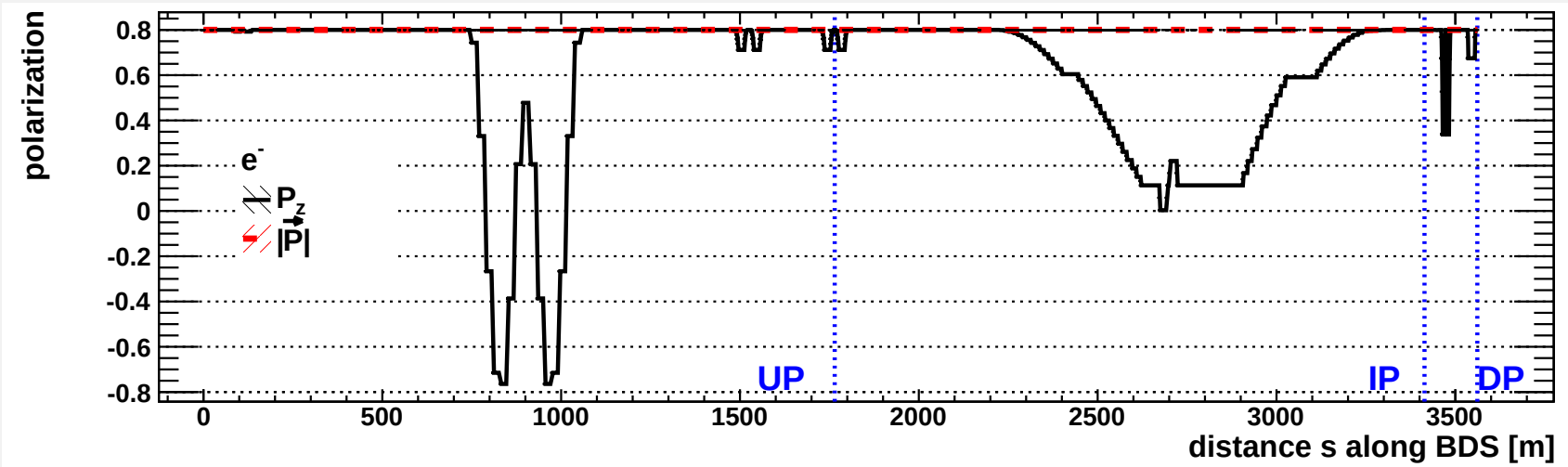

UP/DP: up-/downstream polarimeter

Spin Transport in the BDS: Basic Configuration

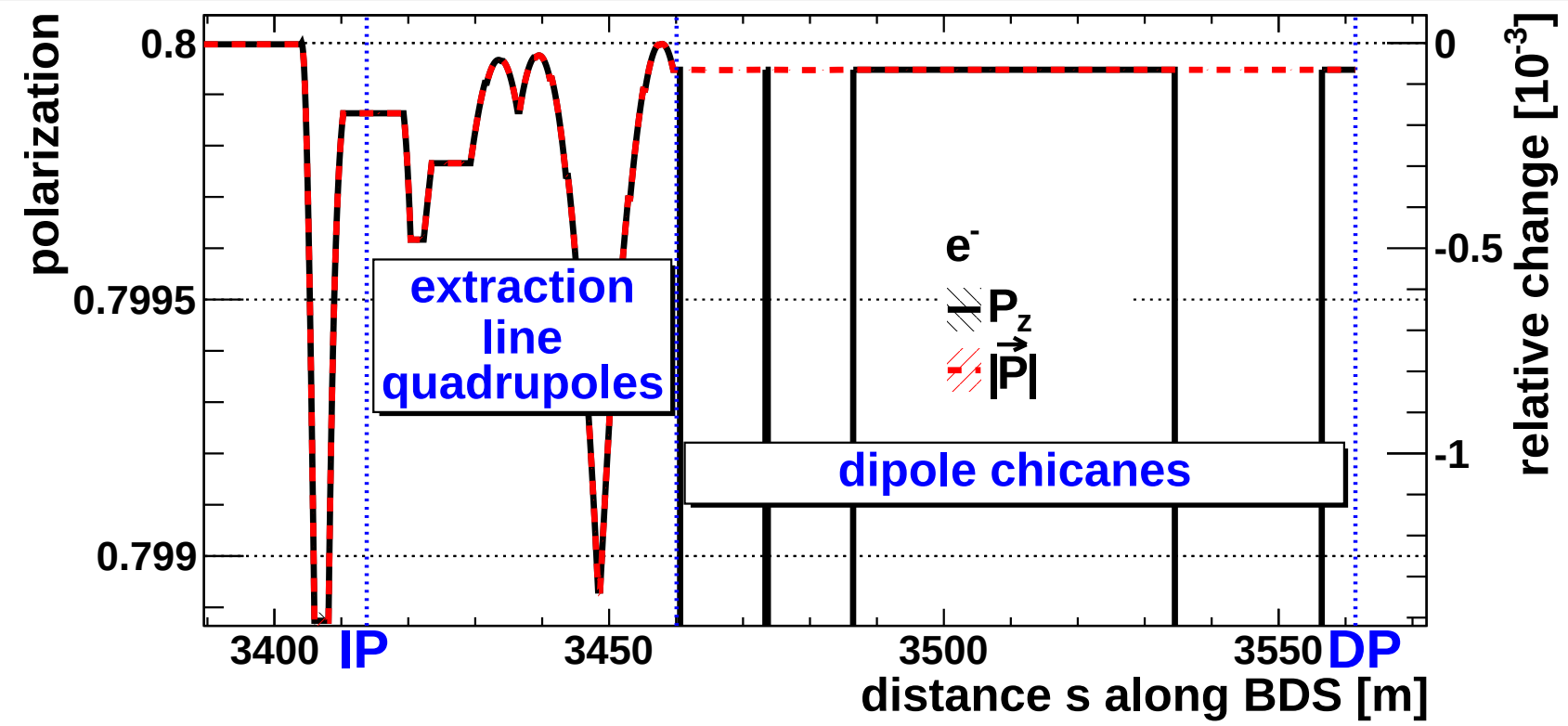

DP: downstream-polarimeter

- Quadrupoles cause spin fan-out
- Changes in $\mathcal{P}_z$ well below 0.1 % without collisions

Factors affecting the spin transport (without collisions)

contribution	uncertainty $[10^{-3}]$
Beam and polarization alignment ($\Delta\vartheta_{\text{bunch}} = 50\,\mu\text{rad}$, $\Delta\vartheta_{\text{pol}} = 25\,\text{mrad}$)	**0.72**
Random misalignments ($10\,\mu\text{m}$)	**0.43**
Variation in beam parameters (few %)	0.03
Bunch rotation (crab cavities)	< 0.01
Detector solenoid	0.01
Synchrotron radiation	0.005
Total (quadratic sum)	0.85

Now: e^+e^- beam collisions

Spin Transport after Collision

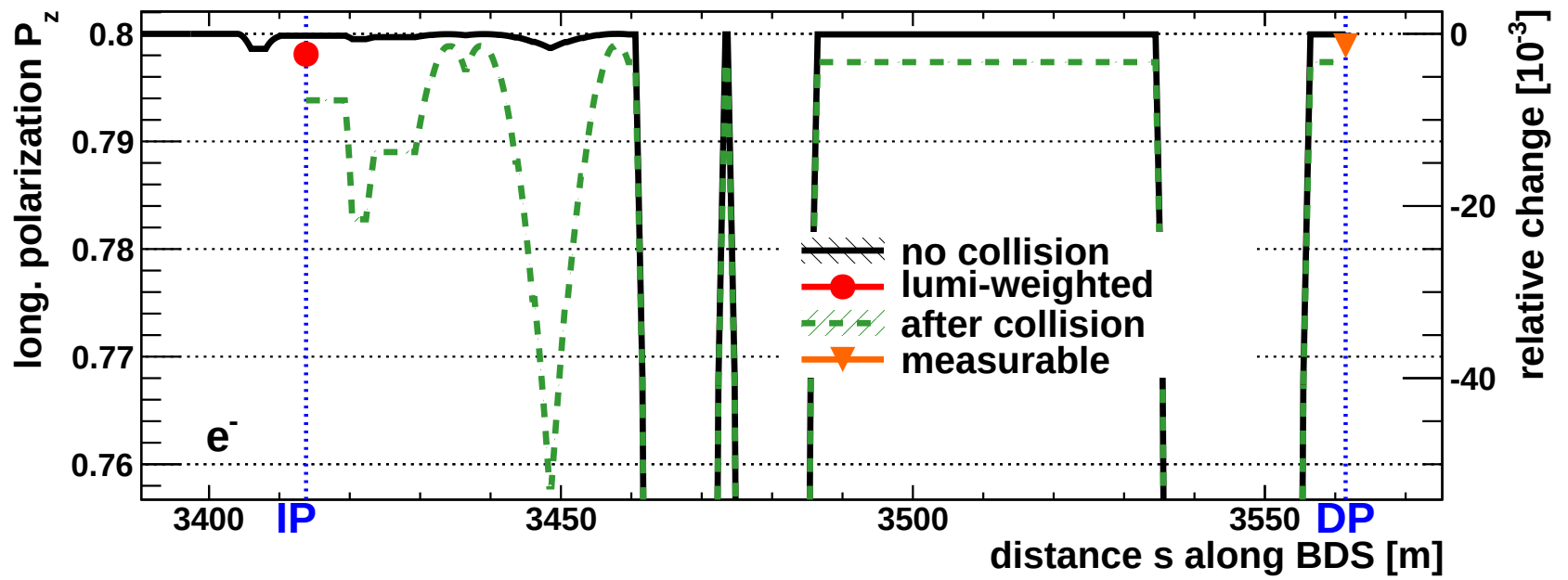

DP: downstream-polarimeter

- **Luminosity-weighted (●): $\mathcal{P}_z$ of the colliding particles**
- Larger angular divergence / energy spread after collision
- Large spin fan-out in extraction line quadrupoles

Spin Transport after Collision

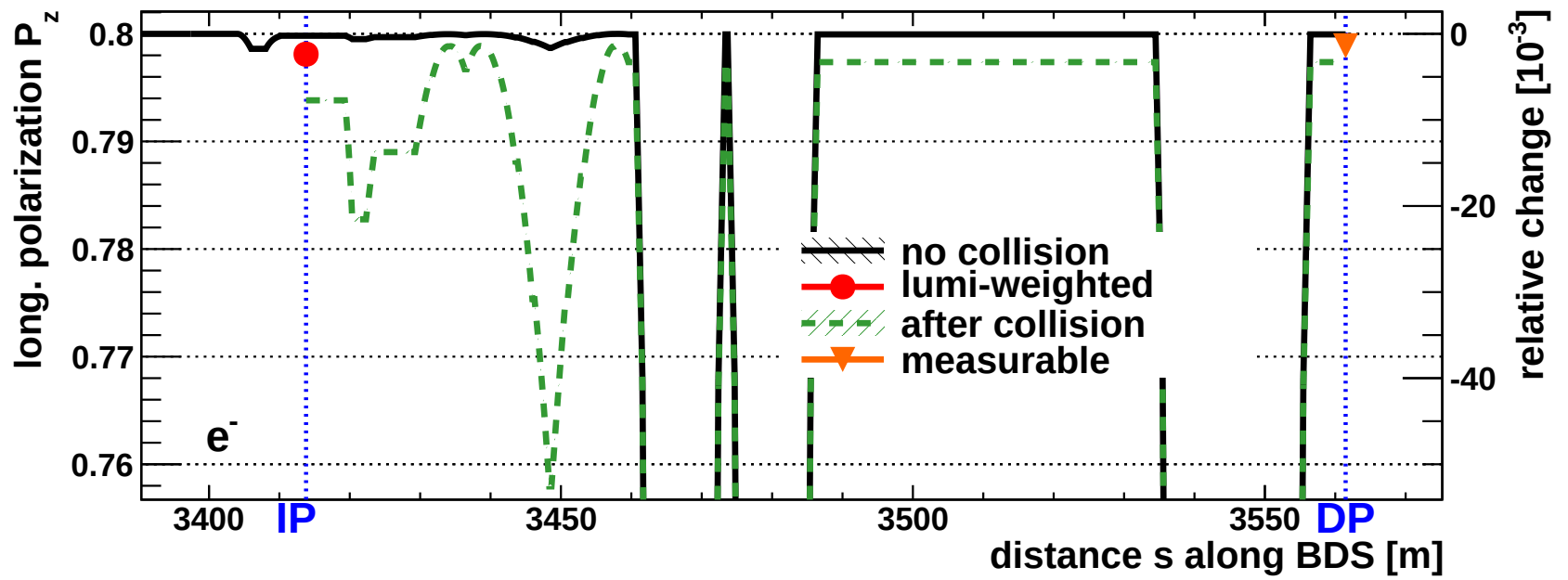

DP: downstream-polarimeter

- **Extraction line design: restore luminosity-weighted $\mathcal{P}_z$ (●) at the downstream polarimeter**
- **Employ spin fan-out**: focus beam at downstream polarimeter with half divergence angle w. r. t. the IP

Spin Transport after Collision

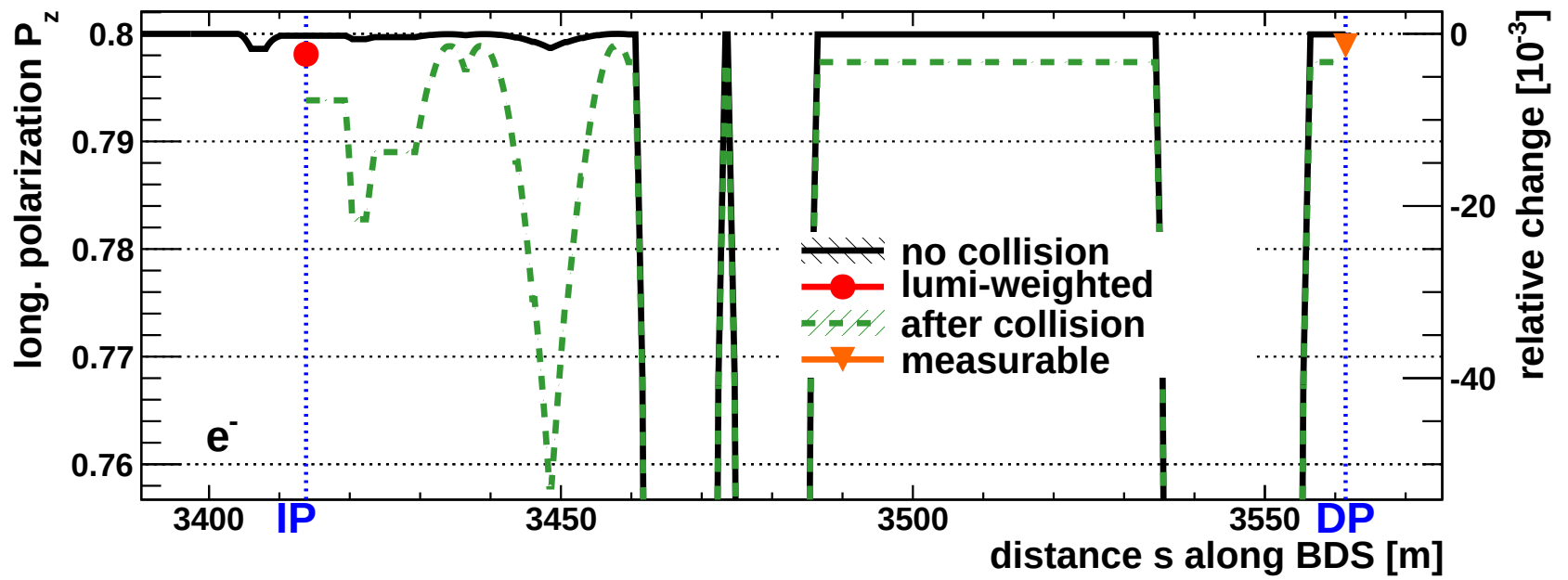

DP: downstream-polarimeter

$$\theta_x \gg \theta_y \quad \Rightarrow \quad \Delta P_z \propto \theta_x^{\,2}$$

$$\Delta P_z^{\text{lum}} \approx \tfrac{1}{4}\Delta P_z \propto \left(\frac{\theta_x}{2}\right)^2$$

Idea: $|R_{22}(\text{IP} \rightarrow \text{DP})| = 0.5 \quad \Rightarrow \quad P_z^{\text{lum}} = P_z^{\text{DP}}$

Further reading: SLAC-PUB-4692, SLAC-PUB-8397

Laser and Particle Bunch at the Downstream Polarimeter

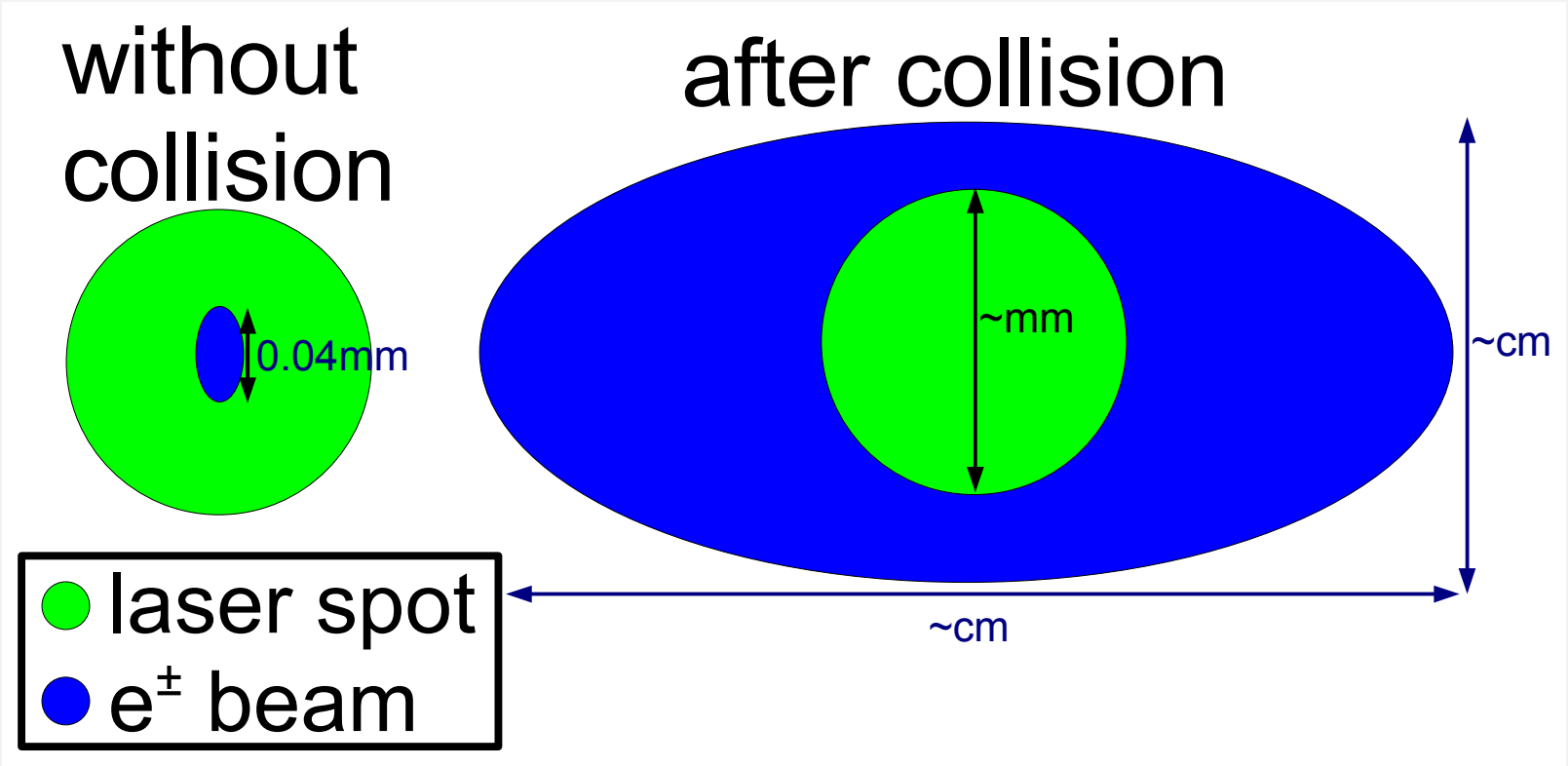

- Without collision: entire beam exposed to laser
- After collision: center of beam exposed to laser
  sample of scattered electrons **representative?**

Downstream Measurement

- Downstream polarimeter located in magnet chicane
  $\Rightarrow$ particle position correlated with energy (**dispersion**)

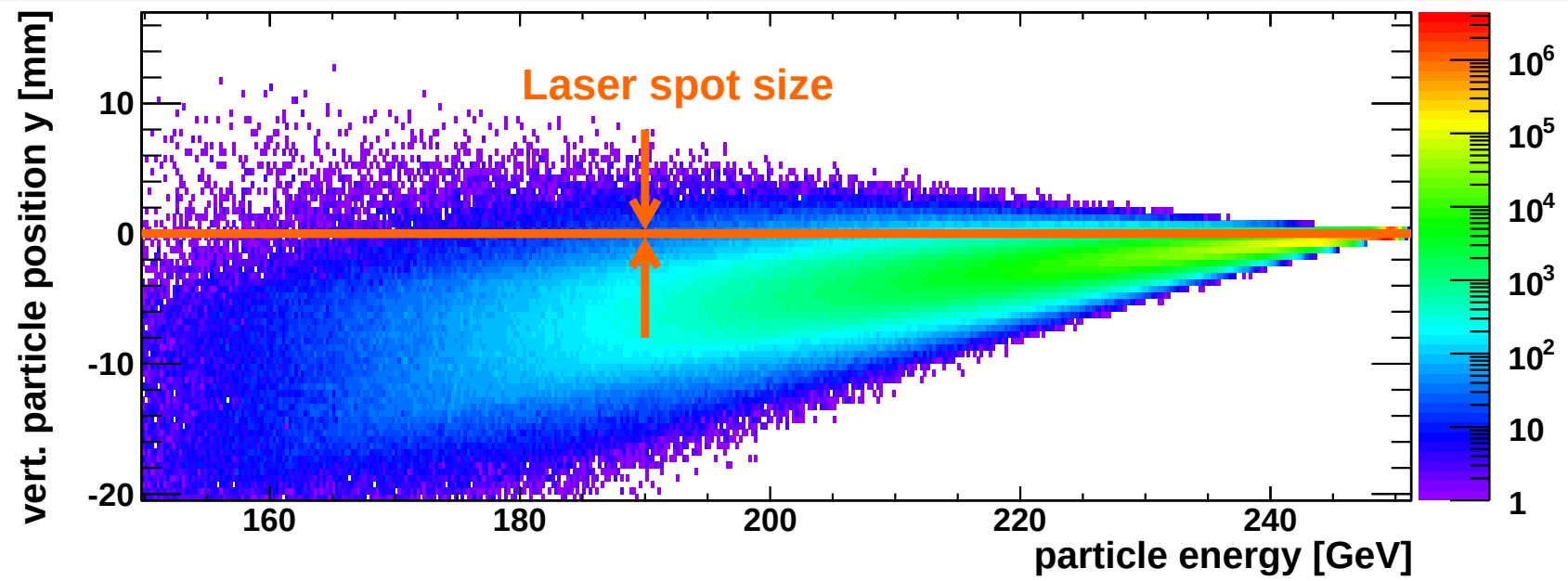

- **Laser spot size** at Compton-IP only $\sim$ **0.1 - 1 mm**

Downstream Measurement

- Beamstrahlung correlates energy and $\mathcal{P}_z$
  $\Rightarrow \mathcal{P}_z$ correlated with particle position
  $\Rightarrow$ **Selective measurement, measurement bias**

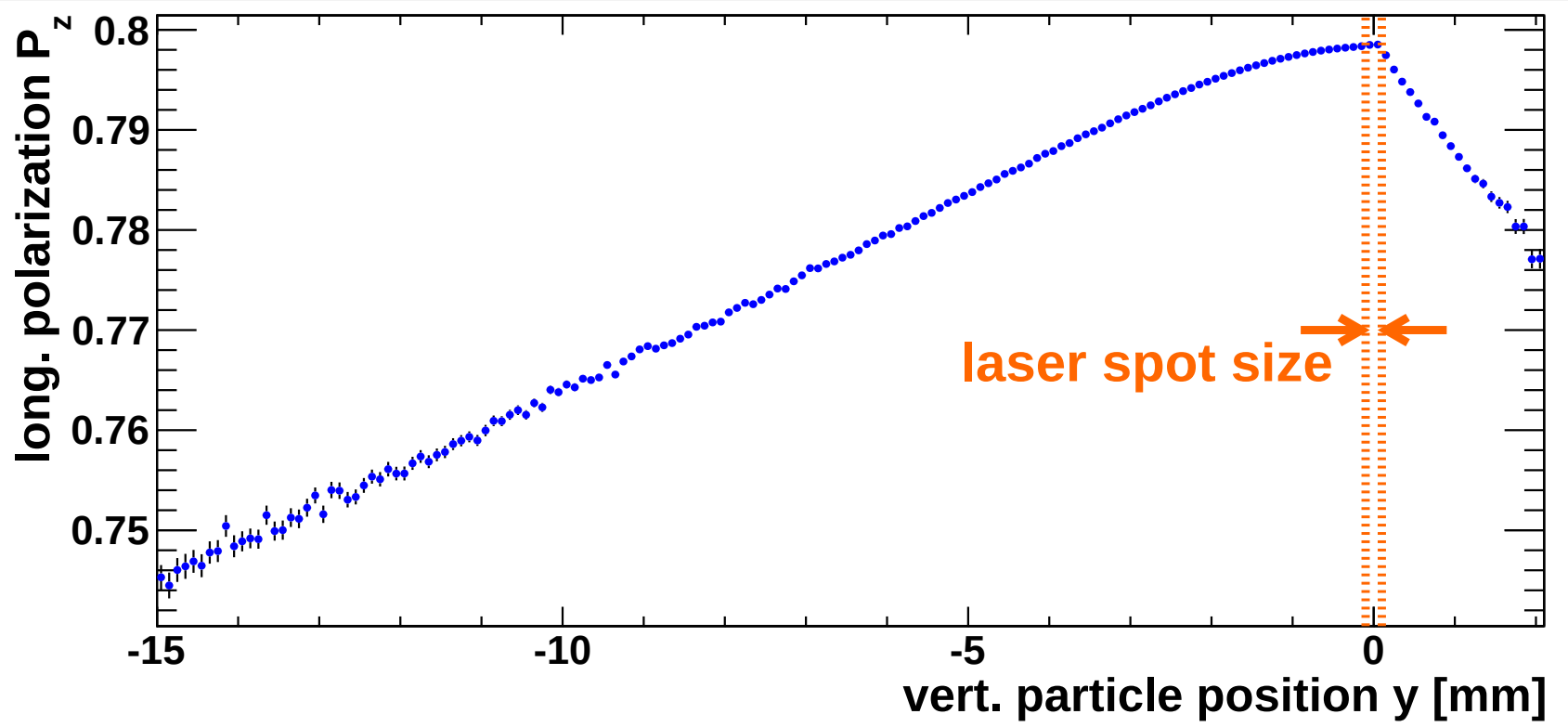

- *Measurable* longitudinal polarization := average $\mathcal{P}_z$ of particles within a given (laser spot) radius

Spin Transport for Different Beam Parameters

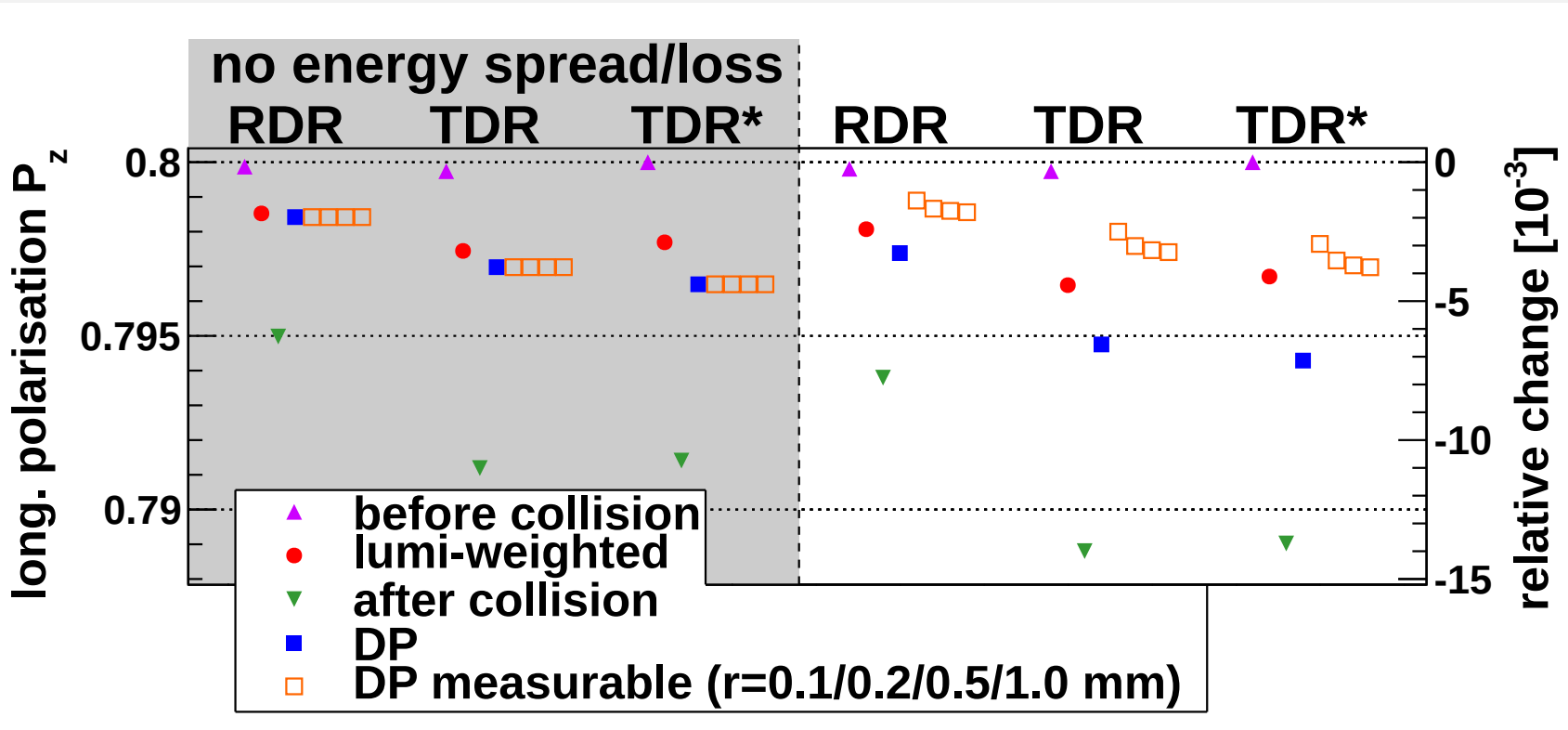

DP: downstream polarimeter

Spin Transport for Different Beam Parameters

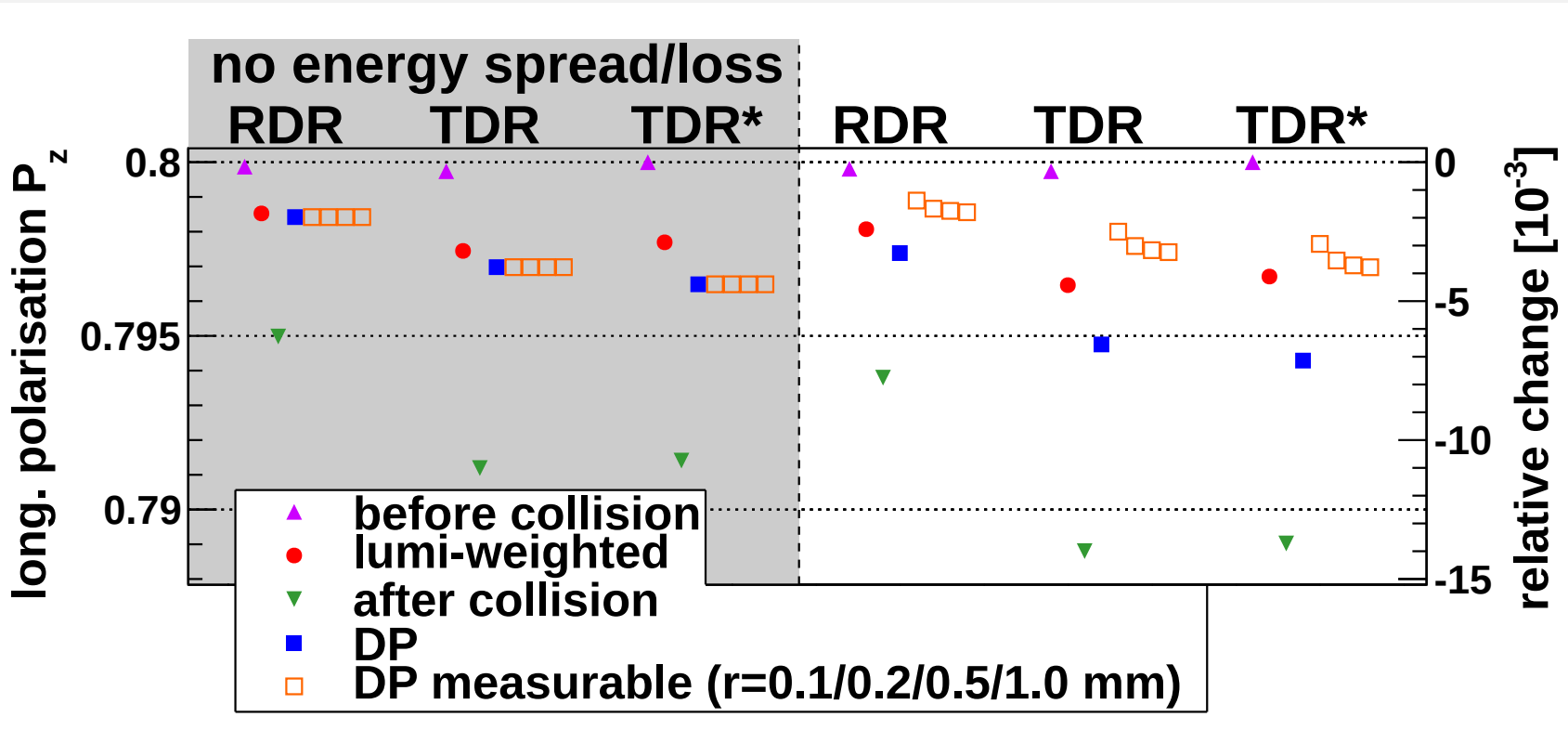

DP: downstream polarimeter

- No energy spread/loss: no discrepancy between measurement (□) and average $\mathcal{P}_z$ (■) at downstream polarimeter
- RDR → TDR: stronger focussing ⇒ higher collision intensity ⇒ larger spin fan-out in collision and afterwards

Spin Transport for Different Beam Parameters

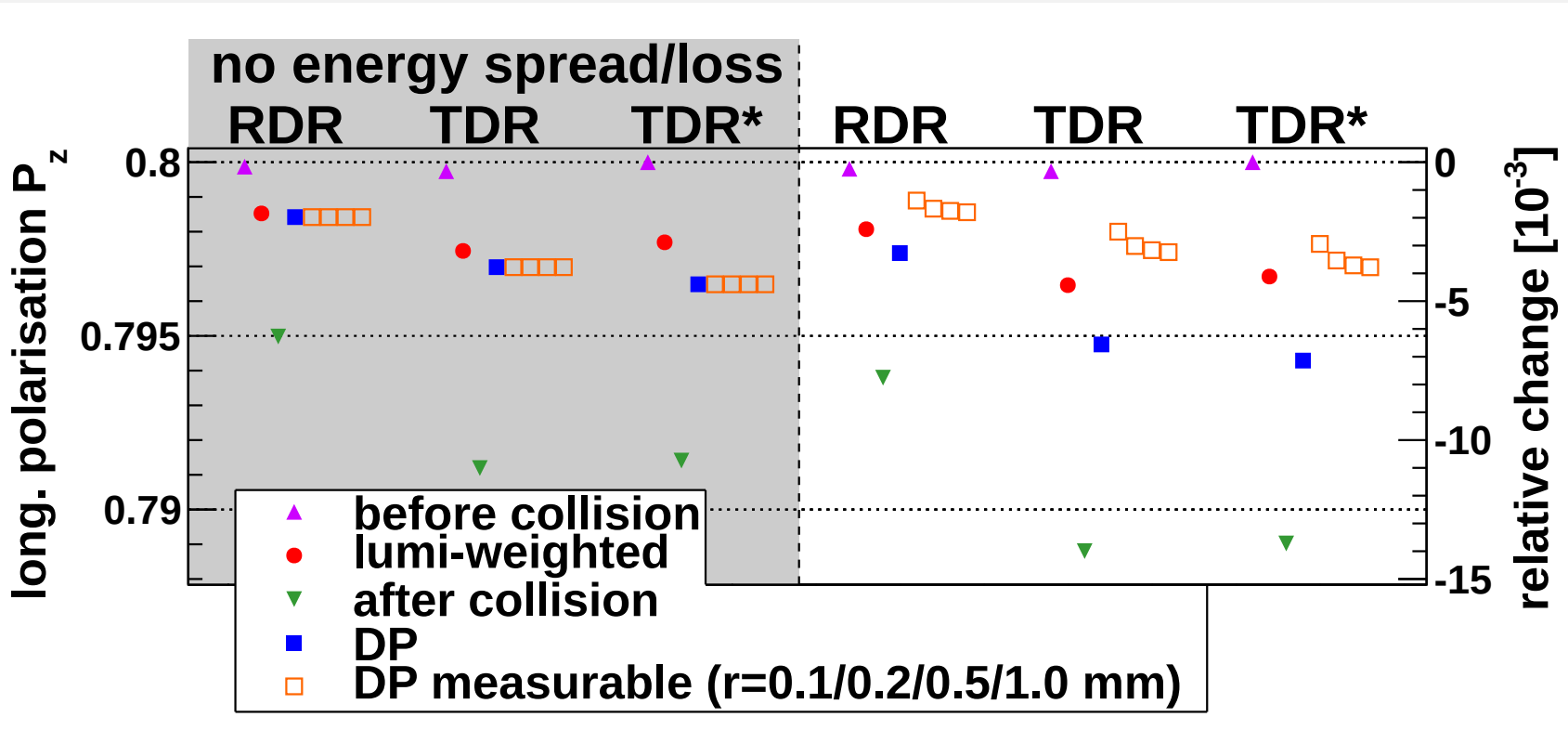

DP: downstream polarimeter

Extraction line design: restore P_z^{lum} (●) at downstream pol. (■)

- Design ($|R_{22}| = 0.5$) assumes $D_x \ll 1$
  $D_x^{\text{RDR}} = 0.17 \qquad D_x^{\text{TDR}} = 0.3$
- More beamstrahlung (not accounted for by design)

Spin Transport for Different Spin Configurations

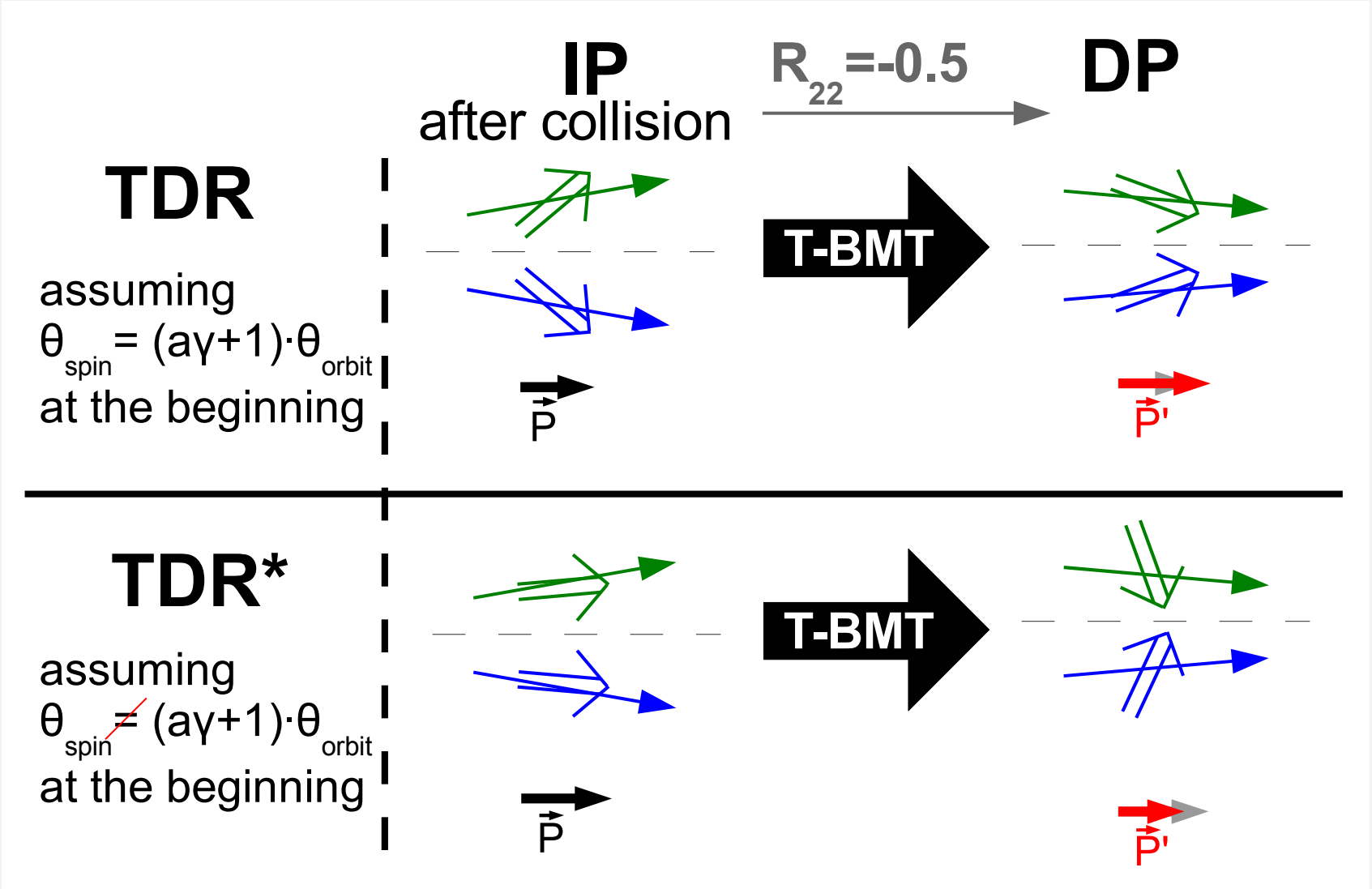

For illustration only. All angles exaggerated. Beamstrahlung effects neglected.

Spin Transport for Different Spin Configurations

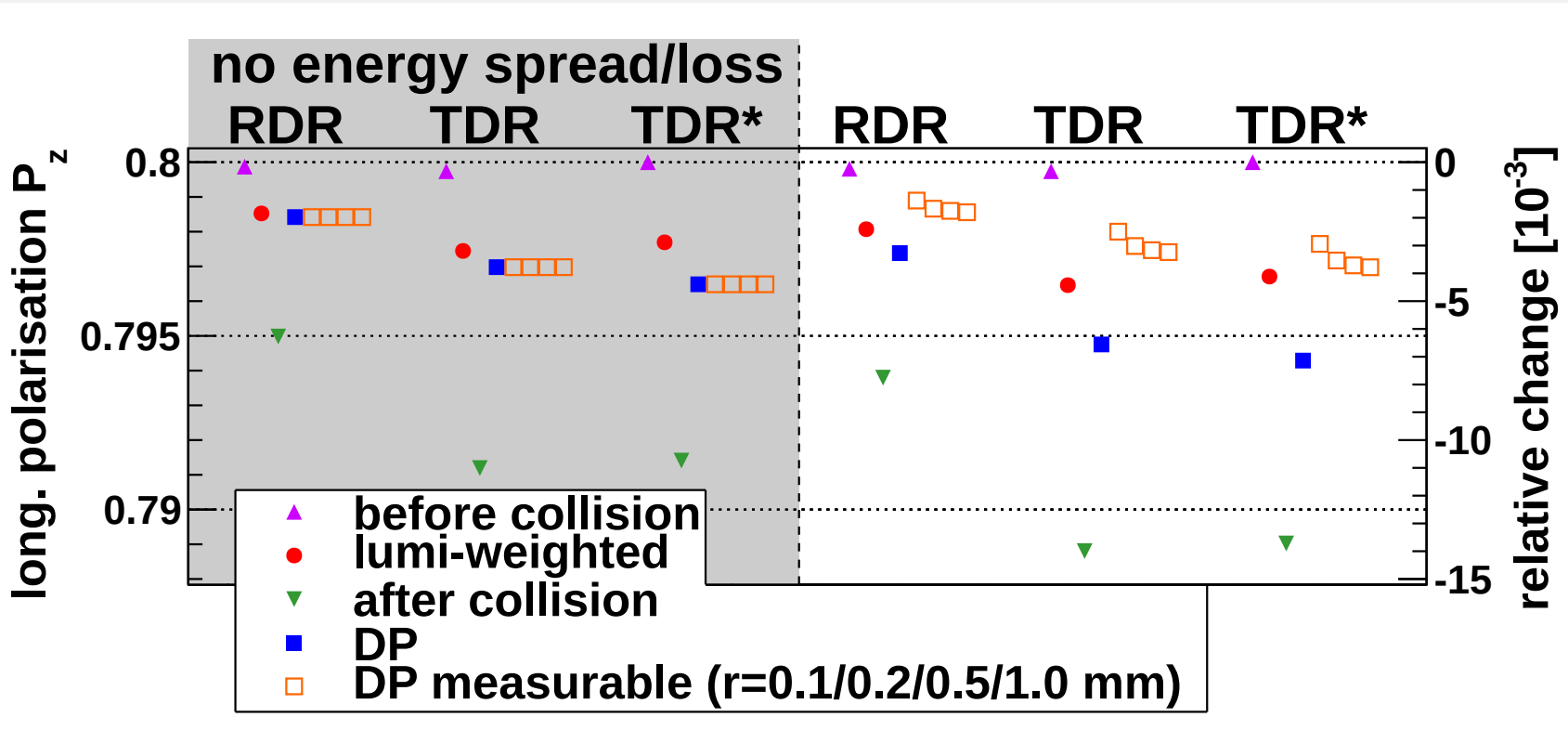

DP: downstream polarimeter

TDR* with respect to TDR:

- All spin vectors parallel before collision, bunch focussed (45 μrad divergence angle)
- Mostly same behaviour in collision (▲, ●, ▼), but different value at downstream polarimeter (■)

Spin Transport for Different Beam Parameters

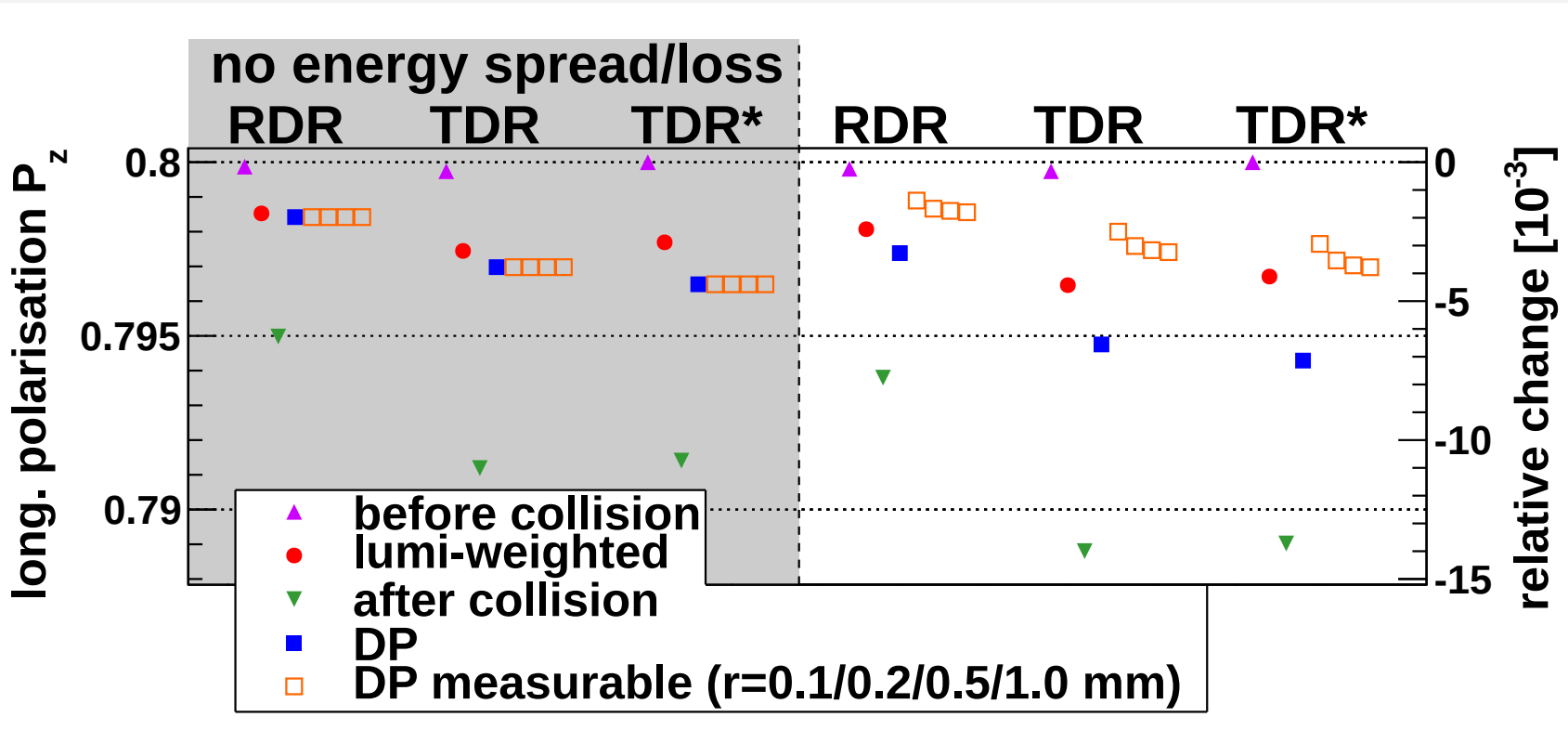

DP: downstream polarimeter

- Polarization varies by several % along the extraction line
- Discrepancies between P_z^{lum} and $\mathcal{P}_z$ at the downstream pol. (●, ■, □) in the range $0.1 - 0.4\,\%$;
  discrepancies cancel partially, but only coincidentally

Conclusions

- Cross-calibration (without collisions) to precision of $< 0.1\,\%$
- Polarization vector alone not sufficient anymore to describe spin configuration of beam:
  - Spin fan-out becomes relevant due to higher measurement precision, higher energy and more intensive collisions
  - How well do we know the initial spin configuration?
    $\rightarrow$ "cradle-to-grave" simulation

Conclusions

- Cross-calibration (without collisions) to precision of $< 0.1\,\%$
- Polarization vector alone not sufficient anymore to describe spin configuration of beam:
  - Spin fan-out becomes relevant due to higher measurement precision, higher energy and more intensive collisions
  - How well do we know the initial spin configuration?
    $\rightarrow$ "cradle-to-grave" simulation
- Extraction line design (restore P_z^{lum} at downstream pol.):
  - Works as foreseen for low-intensity collisions ✓
  - TDR beam parameters: higher intensity $\rightarrow$ larger discrepancies
  - Beamstrahlung not taken into account; D_x no longer $\ll 1$
  - Disrupted beam lets knowledge of the laser spot size/position at the downstream polarimeter become crucial for the measurement precision
  - Larger laser-spot? Drawbacks: required laser power, low-energy tail undesired in polarimeter

Thanks for your attention!

Further reading:

- DESY-THESIS-13-053

  `http://www-library.desy.de/preparch/desy/thesis/desy-thesis-13-053.pdf`

- Publication in preparation

Backup Slides

Differences RDR - TDR

Parameter	symbol		RDR	TDR
Bunches per train			2 625	1 312
Horizontal bunch size	σ_x	[nm]	639	474
Vertical bunch size	σ_y	[nm]	5.7	5.9
Beam energy spread (e^-/e^+)	σ_E/E	[10^{-3}]	1.4/1.0	1.24/0.7
e^+e^- luminosity	$\mathcal{L}$	[$10^{38}\,\mathrm{m}^{-2}\,\mathrm{s}^{-1}$]	2	1.47
incl. waist shift				1.8
Beamstrahlung parameter	$\Upsilon_{\mathrm{global}}$		0.048	0.062

Thomas-Bargmann-Michel-Telegdi (T-BMT) Equation

$$\frac{d}{dt}\vec{S} = \left(\vec{\Omega}_B + \vec{\Omega}_E\right) \times \vec{S}$$

$$\begin{aligned}\vec{\Omega}_B &= -\frac{q}{m\gamma}\left((1+a\gamma)\,\vec{B} - \frac{a\,\vec{p}\cdot\vec{B}}{(\gamma+1)\,m^2c^2}\,\vec{p}\right) \\ &= -\frac{q}{m\gamma}\left((1+a\gamma)\,\vec{B}_\perp \;+\; (1+a)\,\vec{B}_\parallel\right)\end{aligned}$$

$$\vec{\Omega}_E = \frac{q}{m\gamma}\cdot\frac{1}{mc^2}\left(a + \frac{1}{1+\gamma}\right)\,\vec{p}\times\vec{E}$$

Compton Scattering

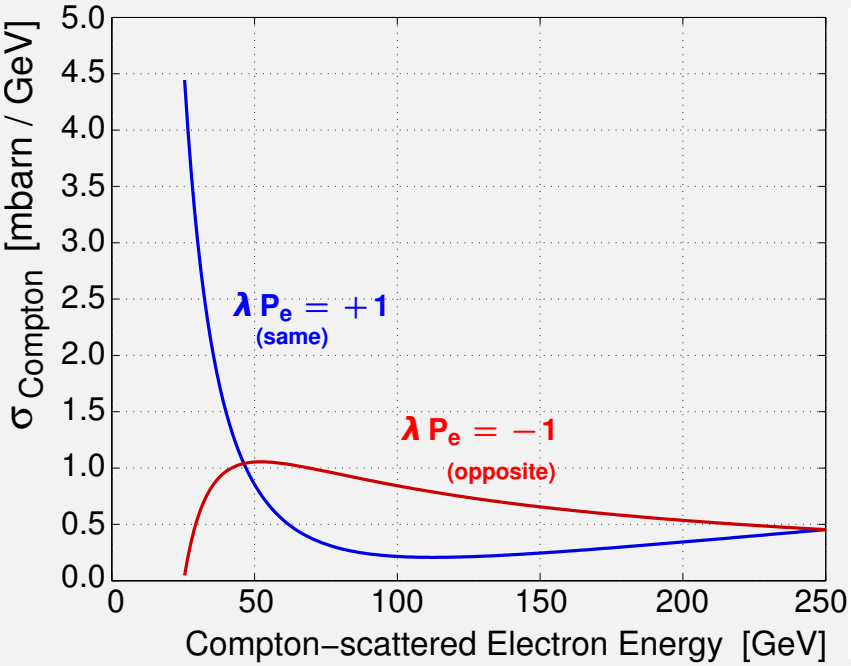

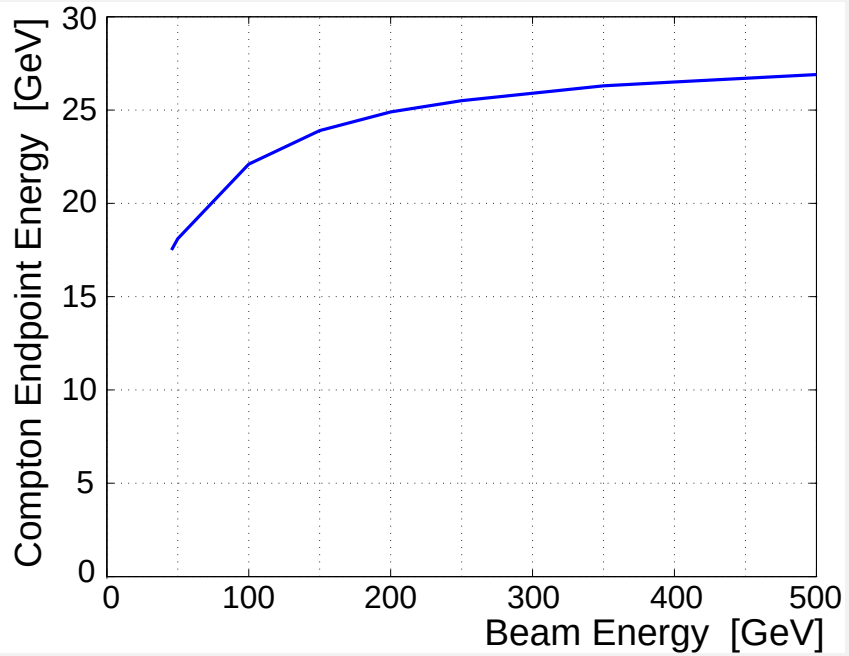

Polarimeter Chicane (upstream)

- Constant magnetic field
- Dispersion (depending on beam energy): 1-11 cm
- Scattering for every bunch per bunch train
- Energy spectrum is polarization-dependent
- Energy distribution $\rightarrow$ spatial distribution
- Cherenkov gas detector counts electrons per channel

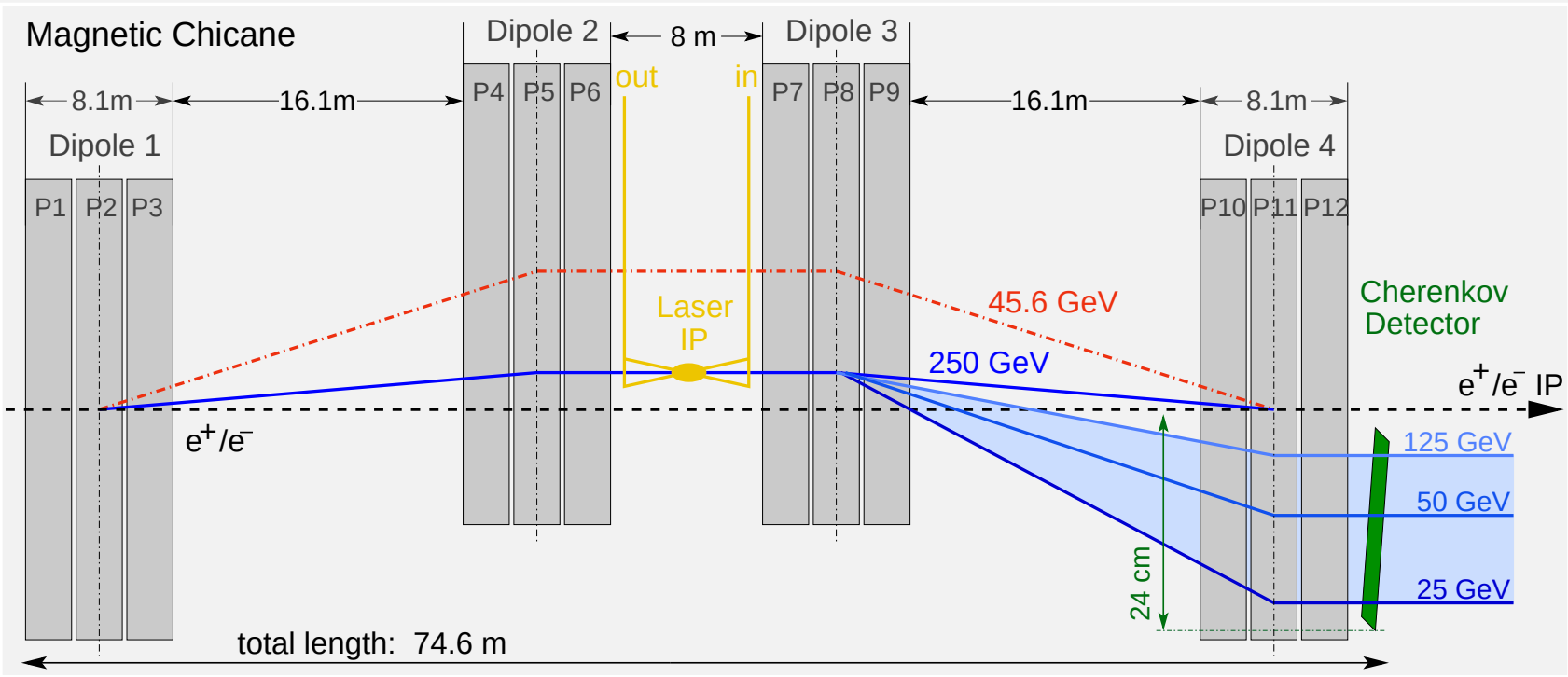

Polarimeter Chicane (downstream)

- Constant magnetic field
- Dispersion (depending on beam energy): 1-11 cm
- Scattering for 3 bunches per bunch train
- Energy spectrum is polarization-dependent
- Energy distribution $\rightarrow$ spatial distribution
- Cherenkov gas detector counts electrons per channel

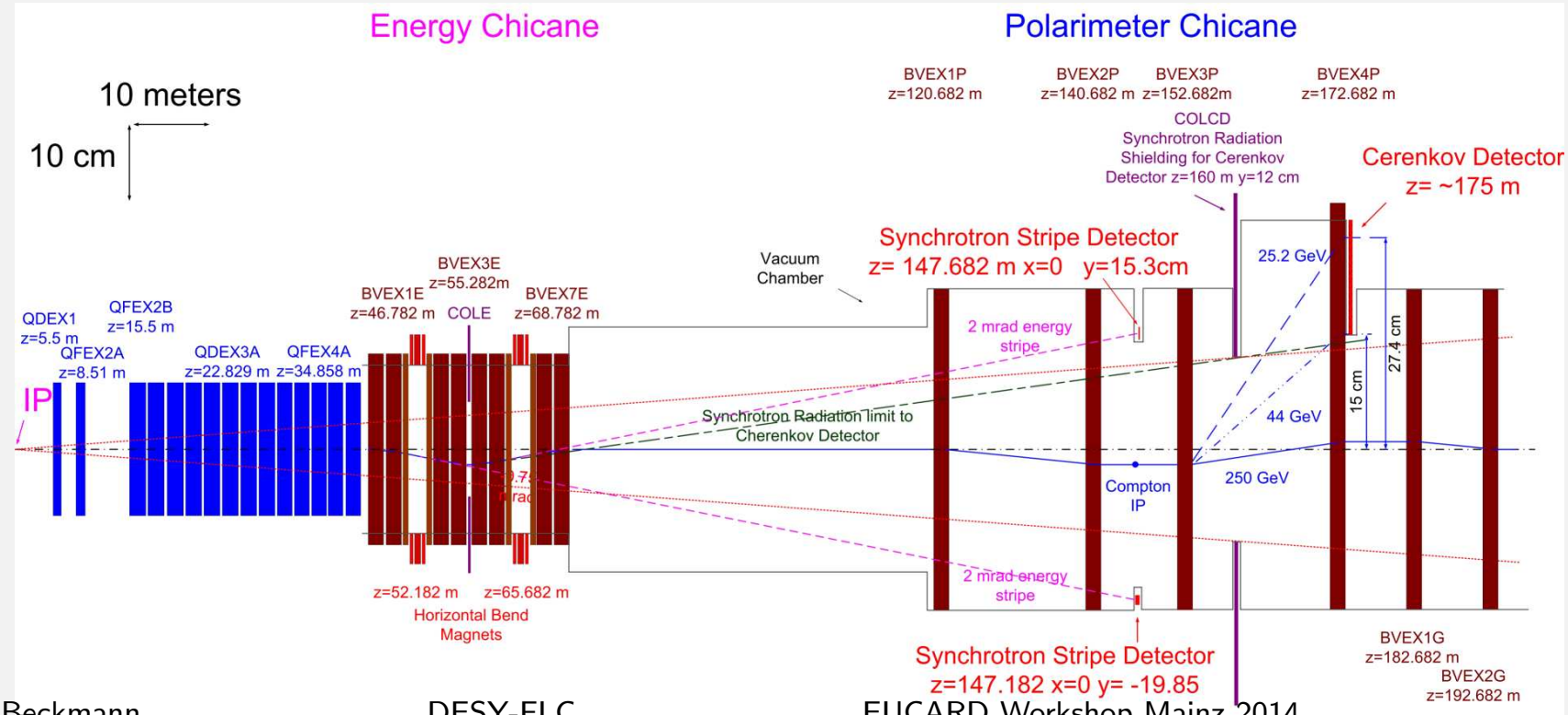

Polarimeter Detector

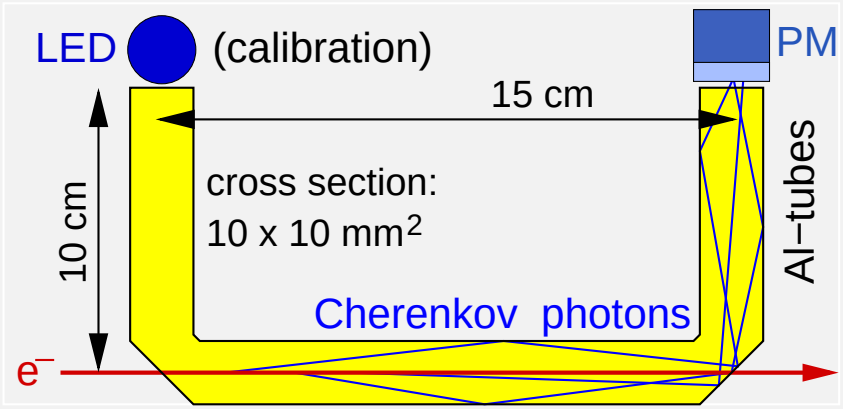

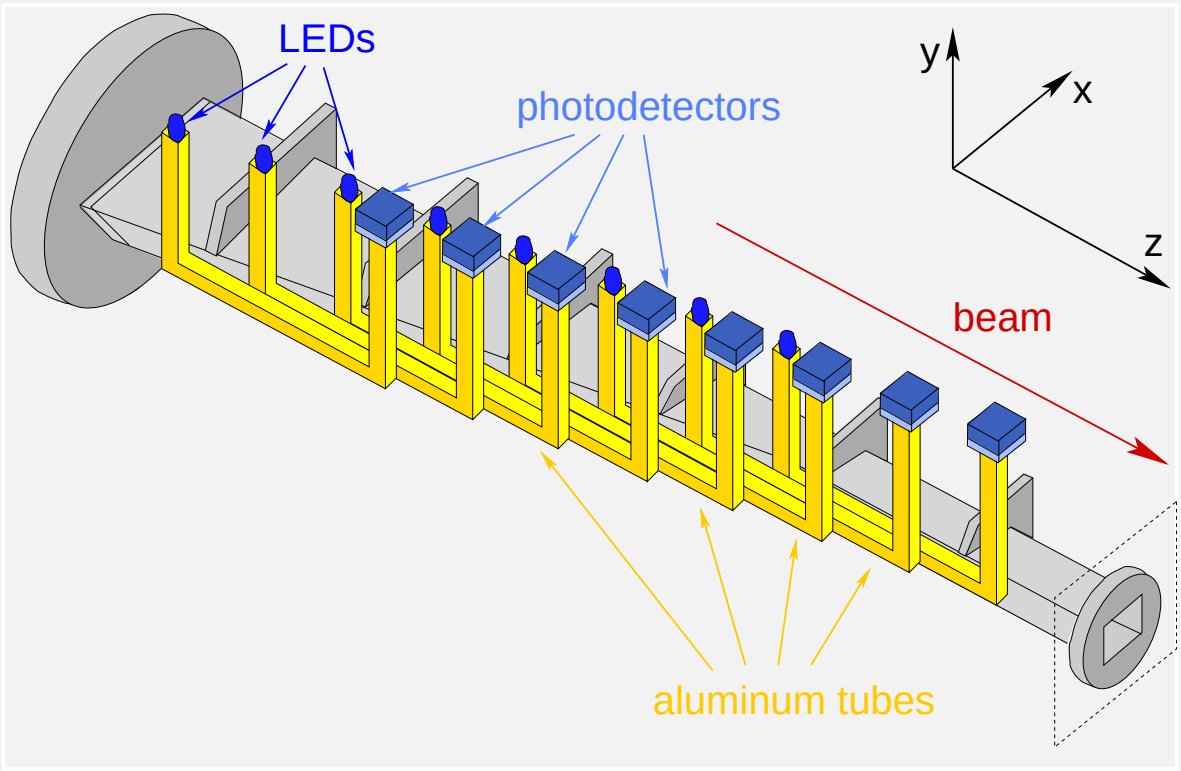

Compton Polarimeters: Systematic Errors

Goal: relative systematic error on measurement $< 0.25\,\%$
(SLD polarimeter: $0.5\,\%$)

- Detector linearity: contribution of $\sim 0.1 - 0.2\,\%$ (goal)
- Laser polarization: $\sim 0.1\,\%$ ✓
- Analyzing power: $\sim 0.1\,\%$ (UP: ✓, DP: ?)
  - Detector alignment: can be determined from data (✓)
    $0.5\,\mathrm{mm}$ precision sufficient
  - Alignment of magnets negligible compared to detector ✓
    Field inhomogeneities? to be investigated
  - Disrupted electron beam at downstream polarimeter:
    - Dependence on laser-spot size and position: ??
    - Beam energy spread no concern for small laser-spot sizes thanks to dispersion ✓

Polarization Measurement at the IP

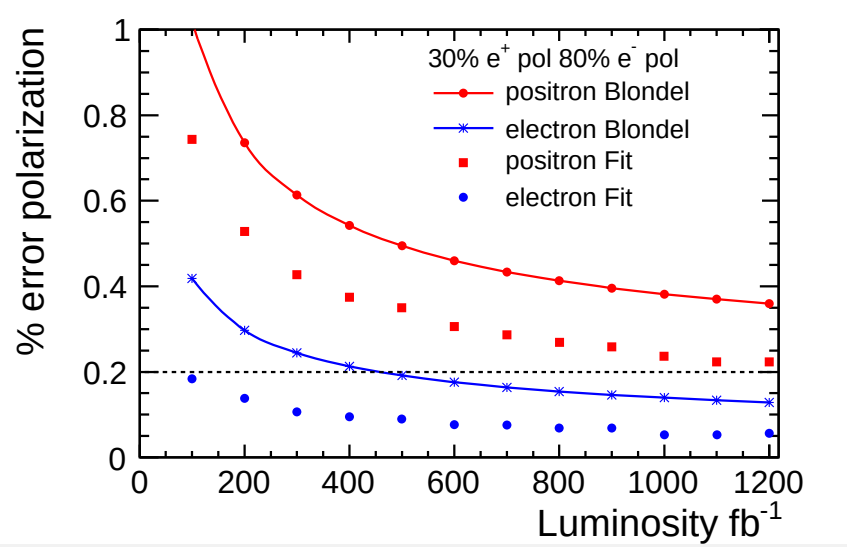

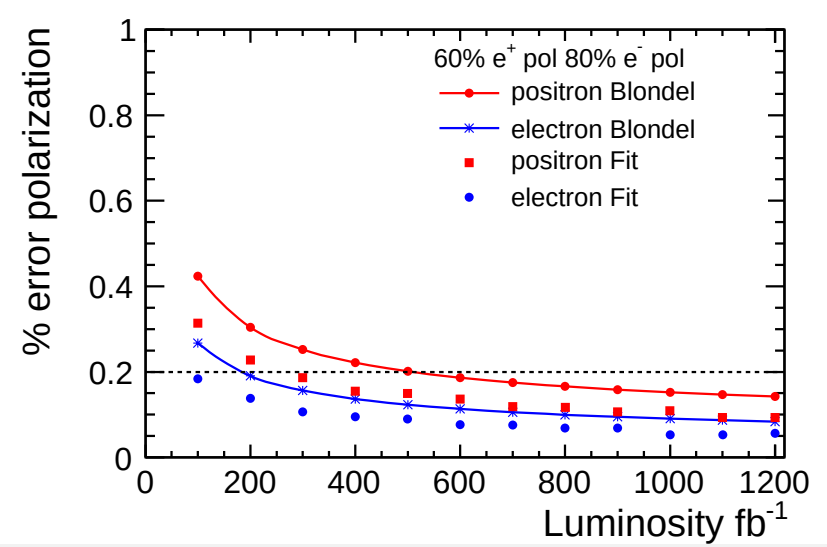

I. Marchesini

Blondel scheme:

$$|\mathcal{P}_z^{\text{lumi}}(e^{\pm})| = \sqrt{\frac{(\sigma_{-+} + \sigma_{+-} - \sigma_{--} - \sigma_{++})(\pm\sigma_{-+} \mp \sigma_{+-} + \sigma_{--} - \sigma_{++})}{(\sigma_{-+} + \sigma_{+-} + \sigma_{--} + \sigma_{++})(\pm\sigma_{-+} \mp \sigma_{+-} - \sigma_{--} + \sigma_{++})}}$$

Polarization Measurement at the IP

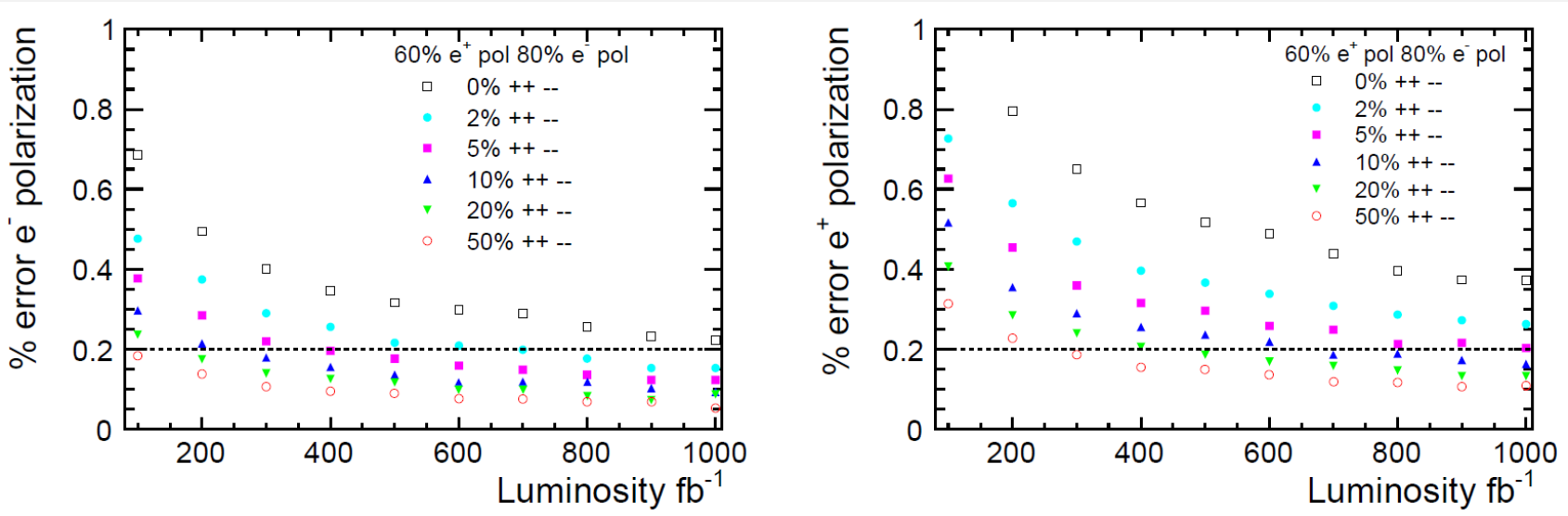

I. Marchesini

Polarization Measurement at the IP

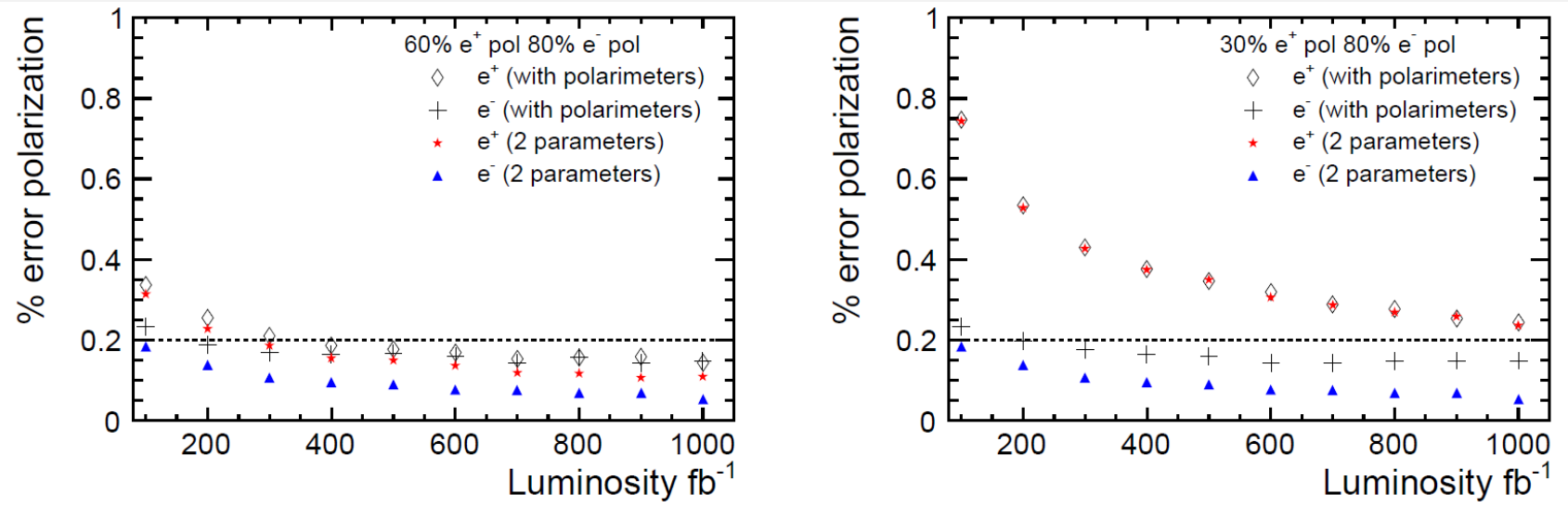

I. Marchesini

Quadrupole Magnet

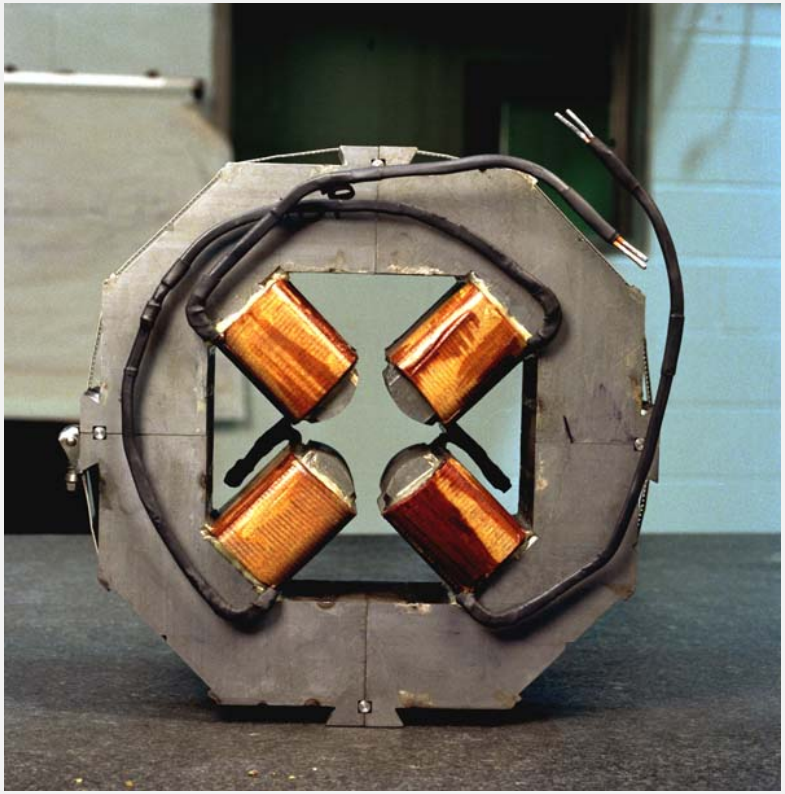

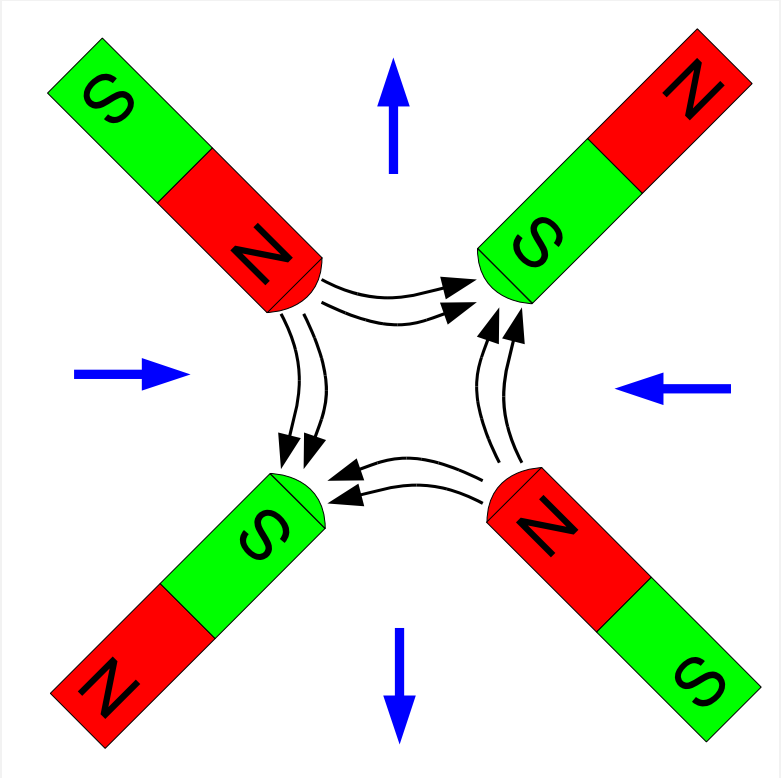

Black arrows: magnetic field lines

Blue arrows: forces on an incoming electron beam

Bunch Rotation at the IP

- Collision under crossing angle of 14 mrad
- Maximize luminosity: rotate bunches using *crab cavities*
- Time-dependent transverse deflection of particles

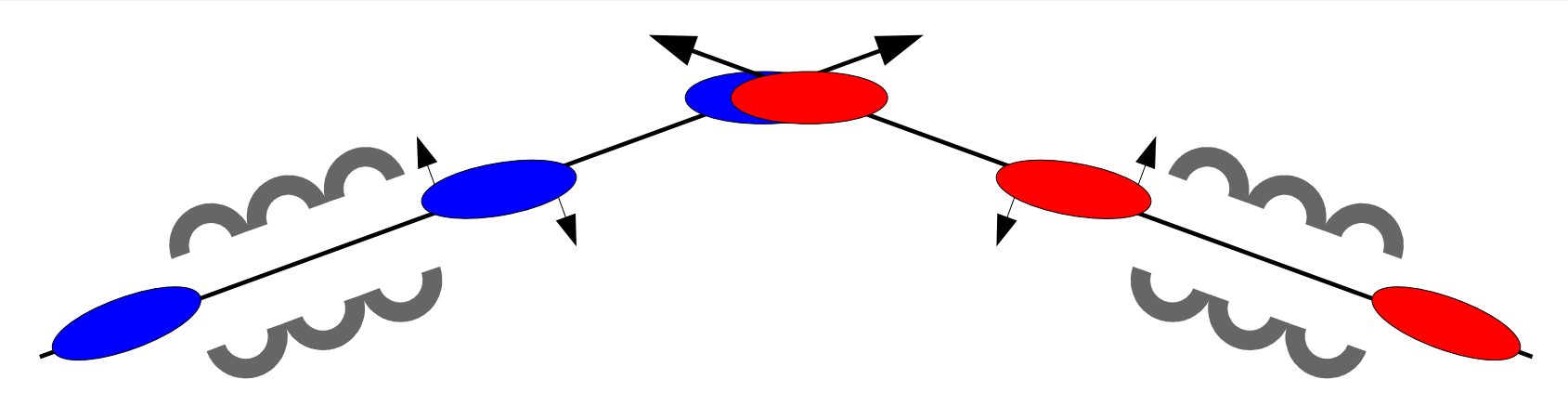

Downstream Pol.: Dispersion w/o Collision

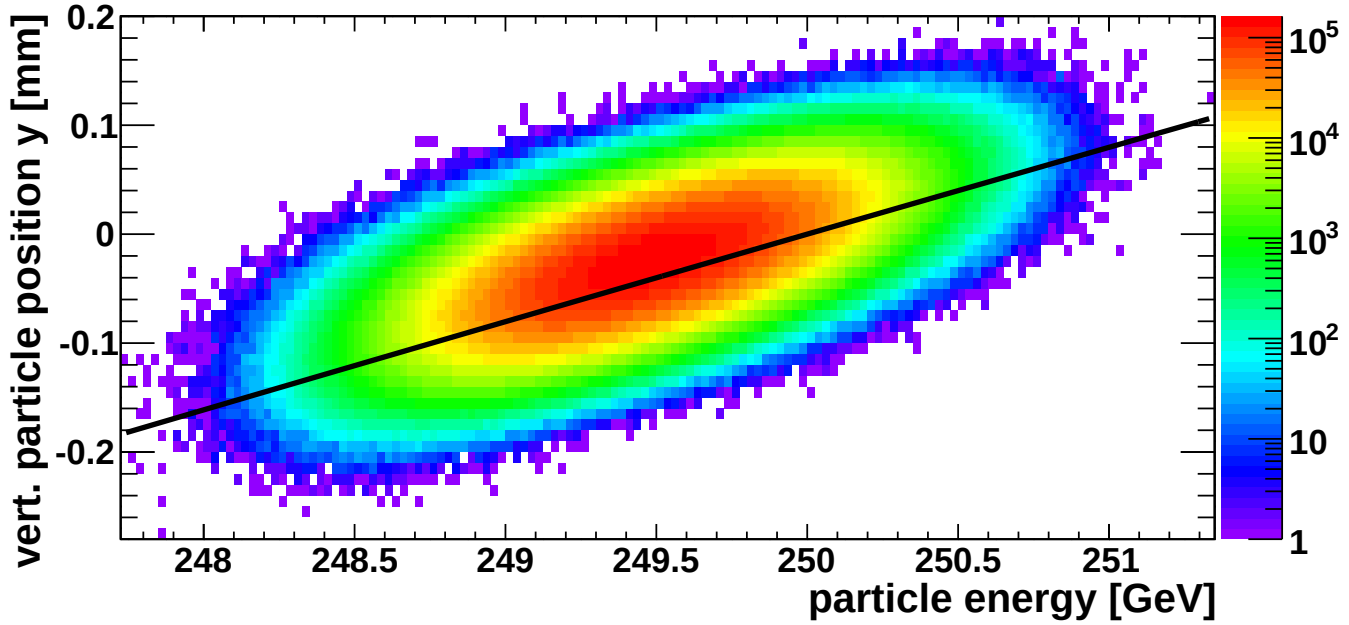

Downstream Pol.: Dispersion after Collision

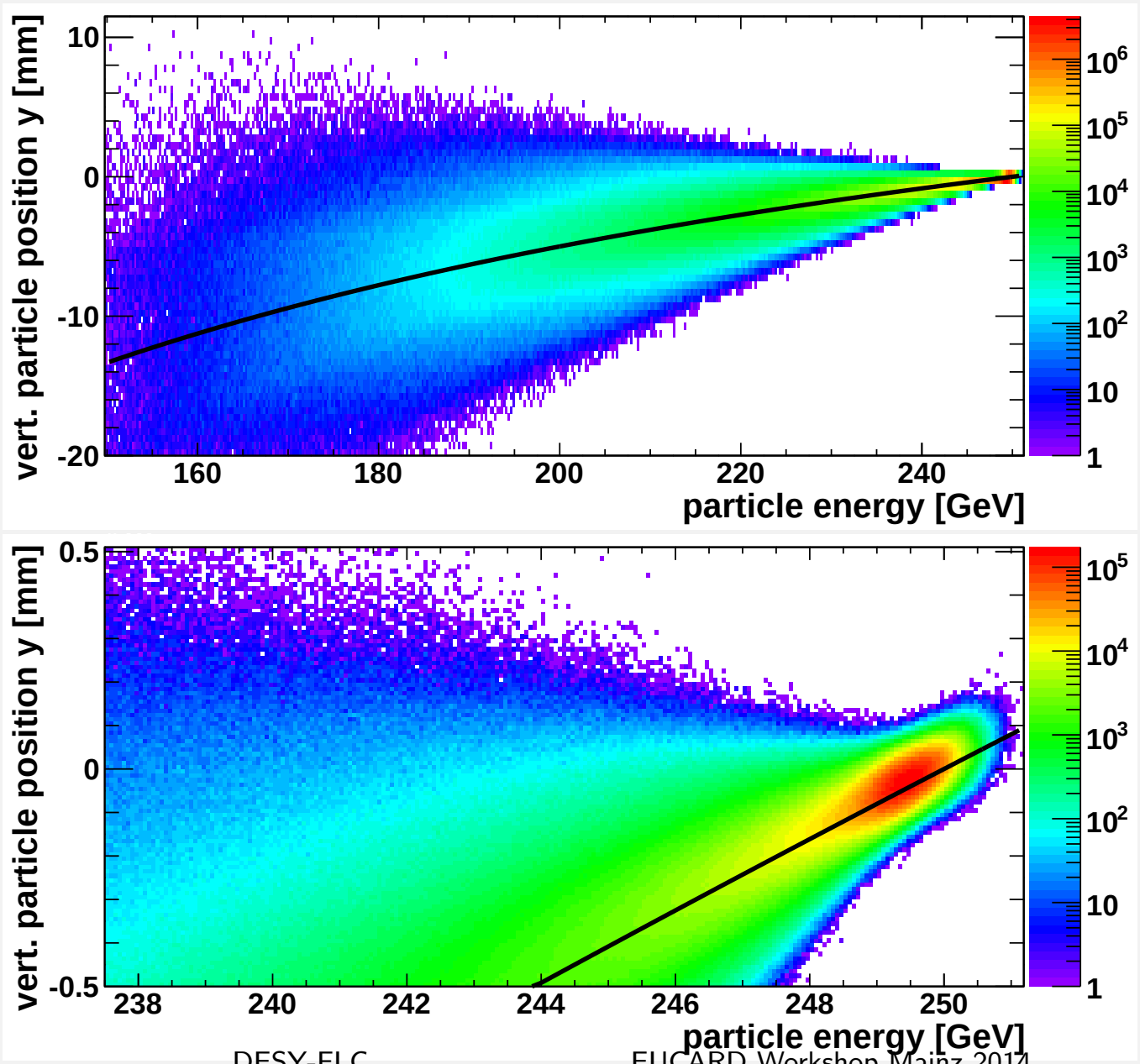

Downstream Measurement

Longitudinal polarization vs. energy at the downstream polarimeter, after collision

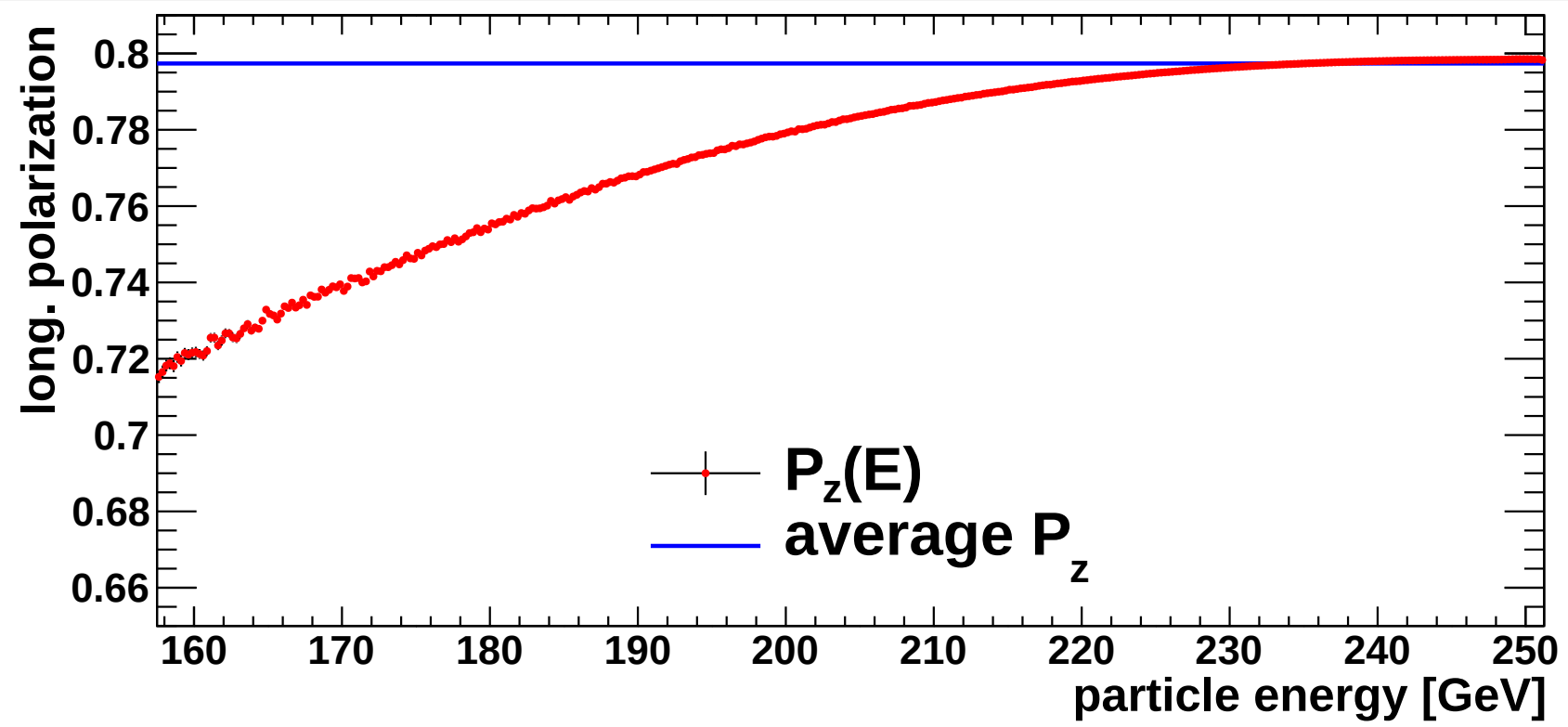

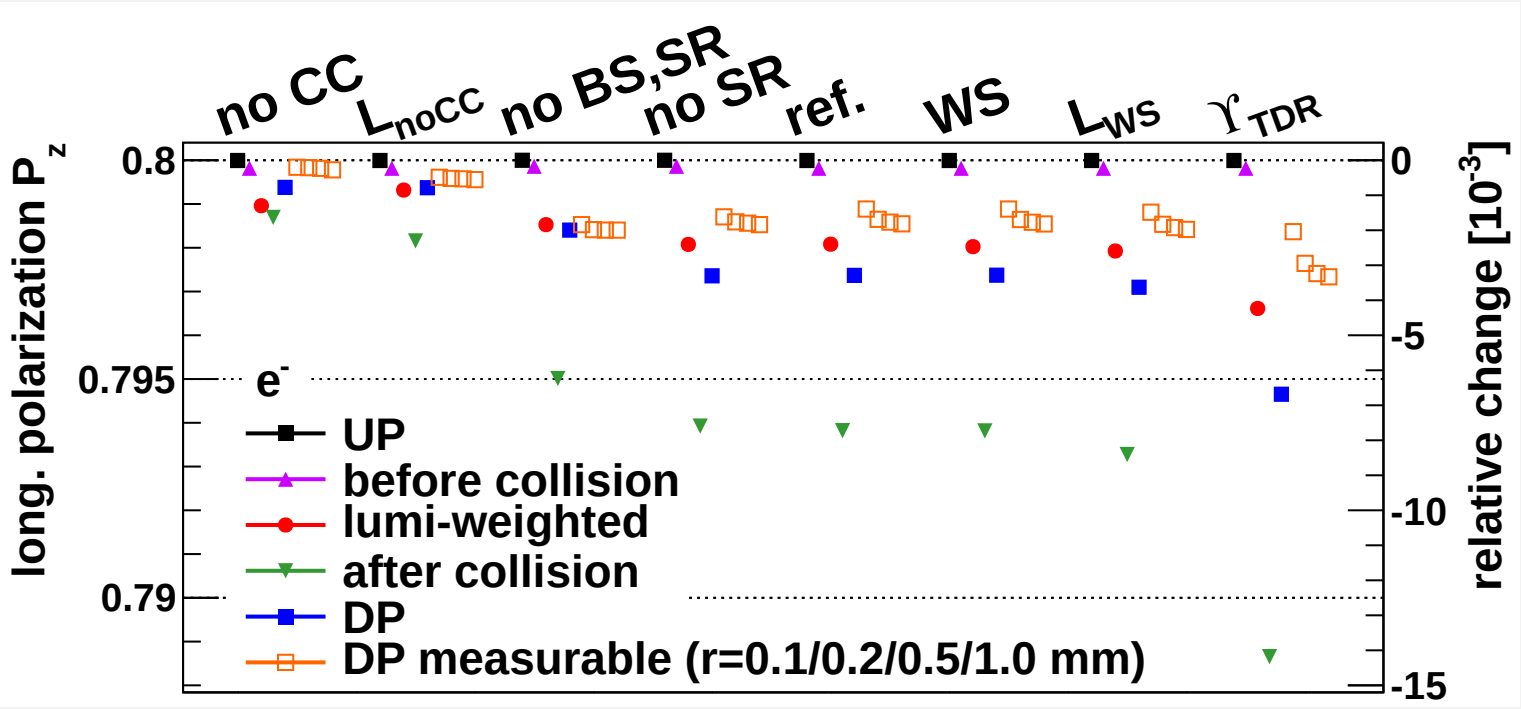
no CC
L_{noCC}
no BS,SR
no SR
ref.
WS
L_{WS}
Υ_{TDR}
long. polarization P_z
0.8
0.795
0.79
e^-
UP
before collision
lumi-weighted
after collision
DP
DP measurable (r=0.1/0.2/0.5/1.0 mm)
0
-5
-10
-15
relative change [10^{-3}]

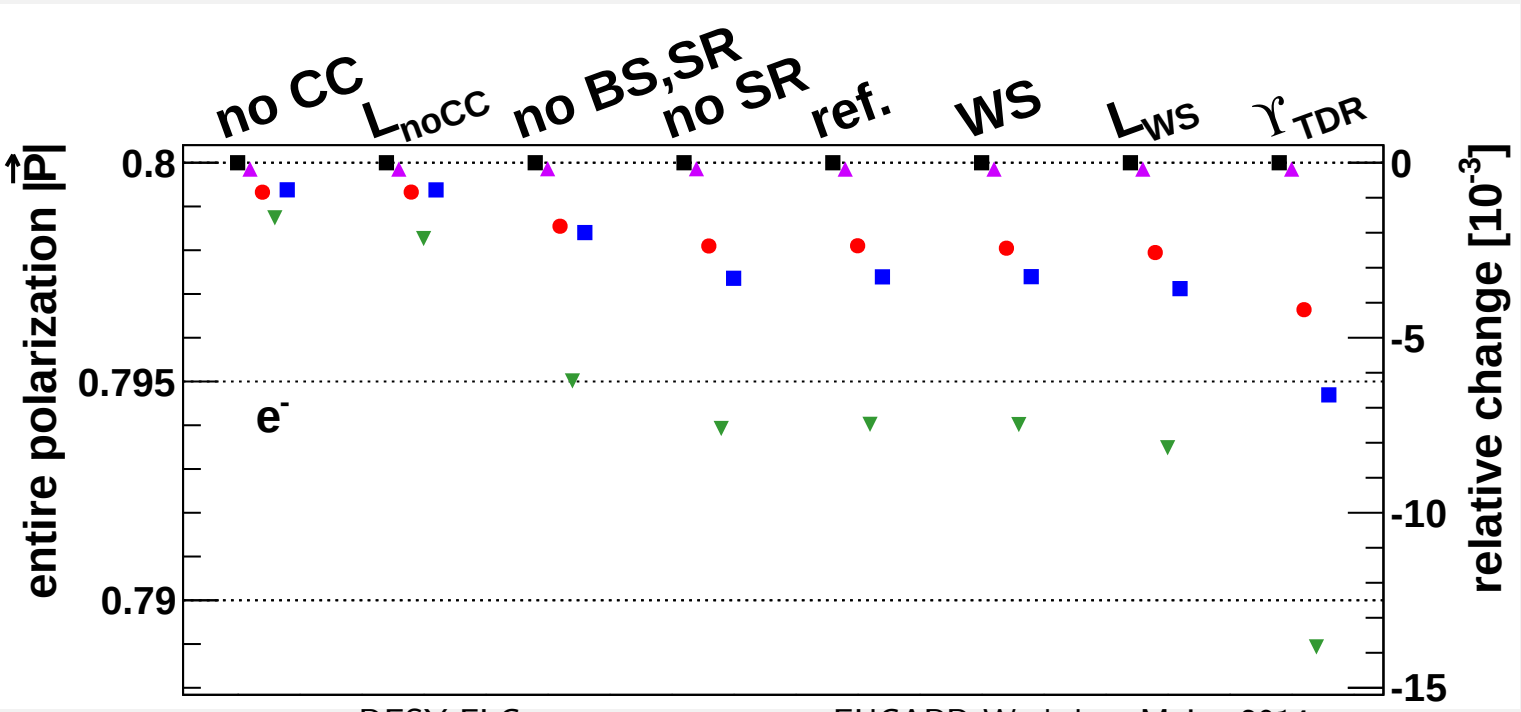
no CC
L_{noCC}
no BS,SR
no SR
ref.
WS
L_{WS}
Υ_{TDR}
entire polarization $|\vec{P}|$
0.8
0.795
0.79
e^-
0
-5
-10
-15
relative change [10^{-3}]

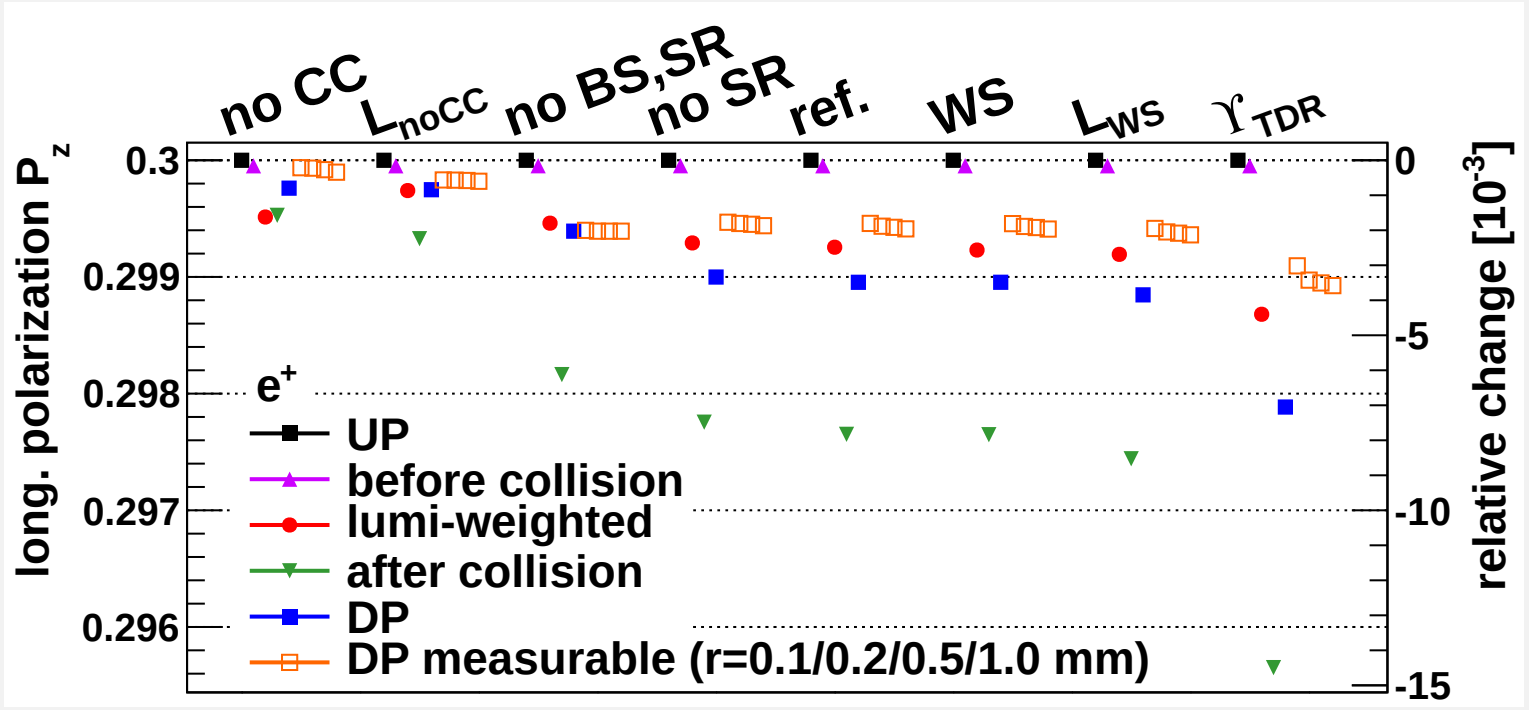
no CC
L_{noCC}
no BS,SR
no SR
ref.
WS
L_{WS}
Υ_{TDR}
long. polarization P_z
relative change [10^{-3}]
0.3
0.299
0.298
0.297
0.296
0
-5
-10
-15
e^+
UP
before collision
lumi-weighted
after collision
DP
DP measurable (r=0.1/0.2/0.5/1.0 mm)

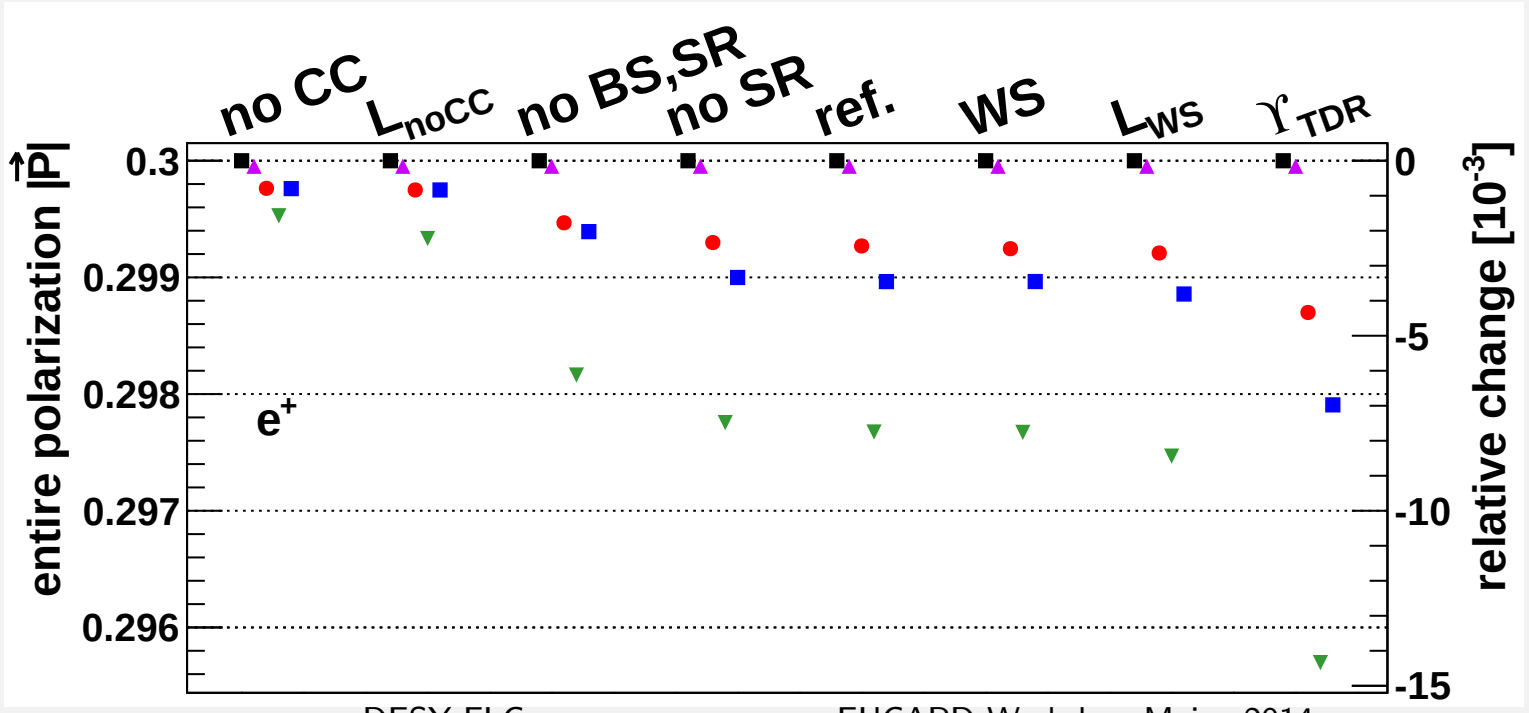
no CC
L_{noCC}
no BS,SR
no SR
ref.
WS
L_{WS}
Υ_{TDR}
entire polarization $|\vec{P}|$
relative change [10^{-3}]
0.3
0.299
0.298
0.297
0.296
0
-5
-10
-15
e^+

Why Polarization?

Electroweak processes: cross sections depend on $\mathcal{P}_z$
e. g. W^+W^- pair production

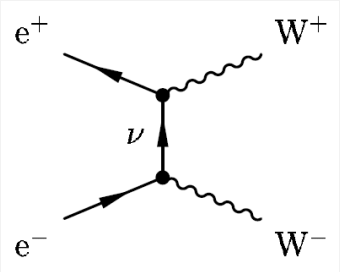

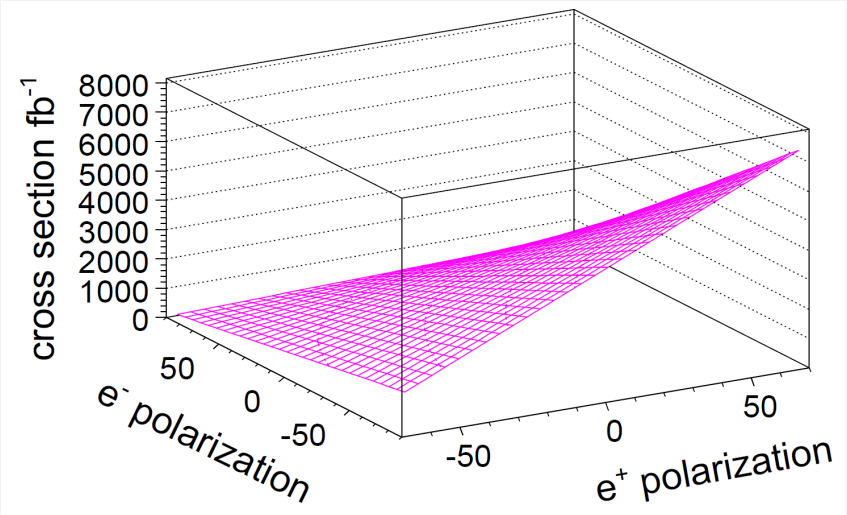

I. Marchesini

Polarized beams

- provide new observables
- can be used to enhance/suppress processes

The International Linear Collider (ILC)

- e^+e^- collider as complement to LHC
- $\sqrt{s} \leq 500\,\text{GeV}$, upgradable to 1 TeV
- Longitudinally polarized beams: $|\mathcal{P}_z(e^-)| = 80\,\%$
  $|\mathcal{P}_z(e^+)| = 30$ to $60\,\%$

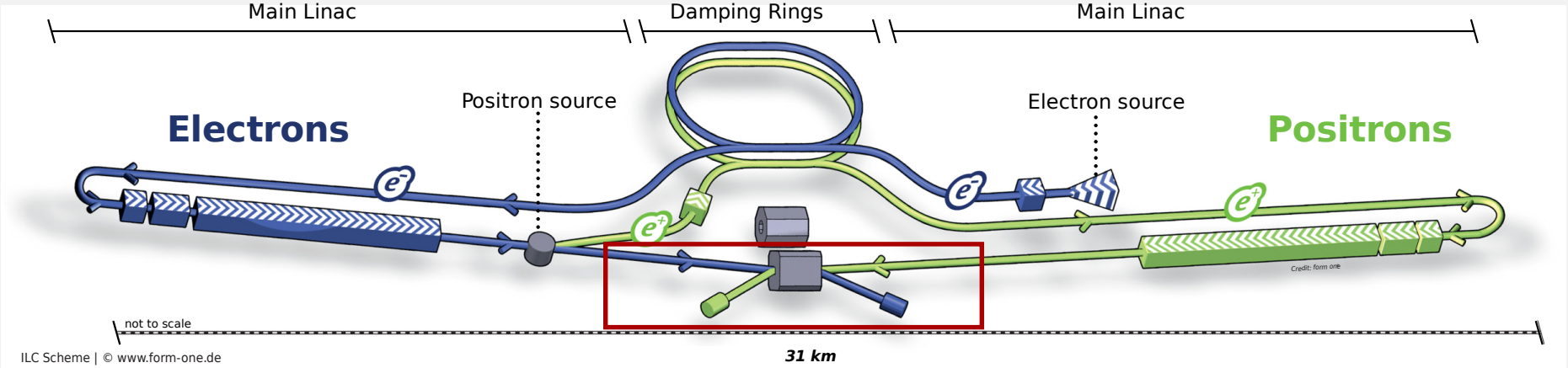

Beam Delivery System